



Analysis of gravity and topography in the GLIMPSE study region: Isostatic compensation and uplift of the Sojourn and Hotu Matua Ridge systems

Nicholas Harmon,¹ Donald W. Forsyth,¹ and Daniel S. Scheirer^{1,2}

Received 27 September 2005; revised 13 July 2006; accepted 26 July 2006; published 25 November 2006.

[1] The Gravity Lineations Intraplate Melting Petrologic and Seismic Expedition (GLIMPSE) Experiment investigated the formation of a series of non-hot spot, intraplate volcanic ridges in the South Pacific and their relationship to cross-grain gravity lineaments detected by satellite altimetry. Using shipboard gravity measurements and a simple model of surface loading of a thin elastic plate, we estimate effective elastic thicknesses ranging from ~ 2 km beneath the Sojourn Ridge to a maximum of 10 km beneath the Southern Cross Seamount. These elastic thicknesses are lower than predicted for the 3–9 Ma seafloor on which the volcanoes lie, perhaps due to reheating and thinning of the plate during emplacement. Anomalously low apparent densities estimated for the Matua and Southern Cross seamounts of 2050 and 2250 kg m⁻³, respectively, probably are artifacts caused by the assumption of only surface loading, ignoring the presence of subsurface loading in the form of underplated crust and/or low-density mantle. Using satellite free-air gravity and shipboard bathymetry, we calculate the age-detrended, residual mantle Bouguer anomaly (rMBA). The rMBA corrects the free-air anomaly for the direct effects of topography, including the thickening of the crust beneath the seamounts and volcanic ridges due to surface loading of the volcanic edifices. There are broad, negative rMBA anomalies along the Sojourn and Brown ridges and the Hotu Matua seamount chain that extend nearly to the East Pacific Rise. These negative rMBA anomalies connect to negative free-air anomalies in the western part of the study area that have been recognized previously as the beginnings of the cross-grain gravity lineaments. Subtracting the topographic effects of surface loading by the ridges and seamounts from the observed topography reveals that the ridges are built on broad bands of anomalously elevated seafloor. This swell topography and the negative rMBA anomalies contradict the predictions of lithospheric cracking models for the origin of gravity lineaments and associated volcanic ridges, favoring models with a dynamic mantle component such as small-scale convection or channelized asthenospheric return flow.

Citation: Harmon, N., D. W. Forsyth, and D. S. Scheirer (2006), Analysis of gravity and topography in the GLIMPSE study region: Isostatic compensation and uplift of the Sojourn and Hotu Matua Ridge systems, *J. Geophys. Res.*, *111*, B11406, doi:10.1029/2005JB004071.

1. Introduction

[2] Satellite altimetry revealed a series of free-air anomaly gravity lineaments in the South Pacific beginning a few hundred kilometers from the East Pacific Rise (EPR) and extending westward in the direction of absolute plate motion (APM) of the Pacific plate in the hot spot coordinate frame [Haxby and Weissel, 1986]. The lineaments have a peak-to-peak amplitude of 5 to 20 mGal and an initial dominant wavelength on the order of 170–200 km that increases somewhat to the west (Figure 1), although a range

of wavelengths is present in all ages of seafloor [Moriceau and Fleitout, 1989; Baudry and Kroenke, 1991; Maia and Diamant, 1991; Cazenave et al., 1992; Fleitout and Moriceau, 1992; Wessel et al., 1994; Cazenave et al., 1995; Wessel et al., 1996; Marquart et al., 1999]. Bathymetric surveying and higher resolution altimetry identified sets of narrow, en echelon, volcanic ridges also trending in the direction of absolute plate motion, coincident with the lows of some of the gravity lineaments [Winterer and Sandwell, 1987; McAdoo and Sandwell, 1989; Shen et al., 1993; Sandwell et al., 1995; Scheirer et al., 1996, 1998]. Radiometric dating of the Puka Puka ridges showed the age progression to be inconsistent with a fixed hot spot origin [Sandwell et al., 1995]. The gravity lineaments were initially attributed to small-scale convective rolls aligned by the motion of the plate

¹Department of Geological Sciences, Brown University, Providence, Rhode Island, USA.

²Now at U.S. Geological Survey, Menlo Park, California, USA.

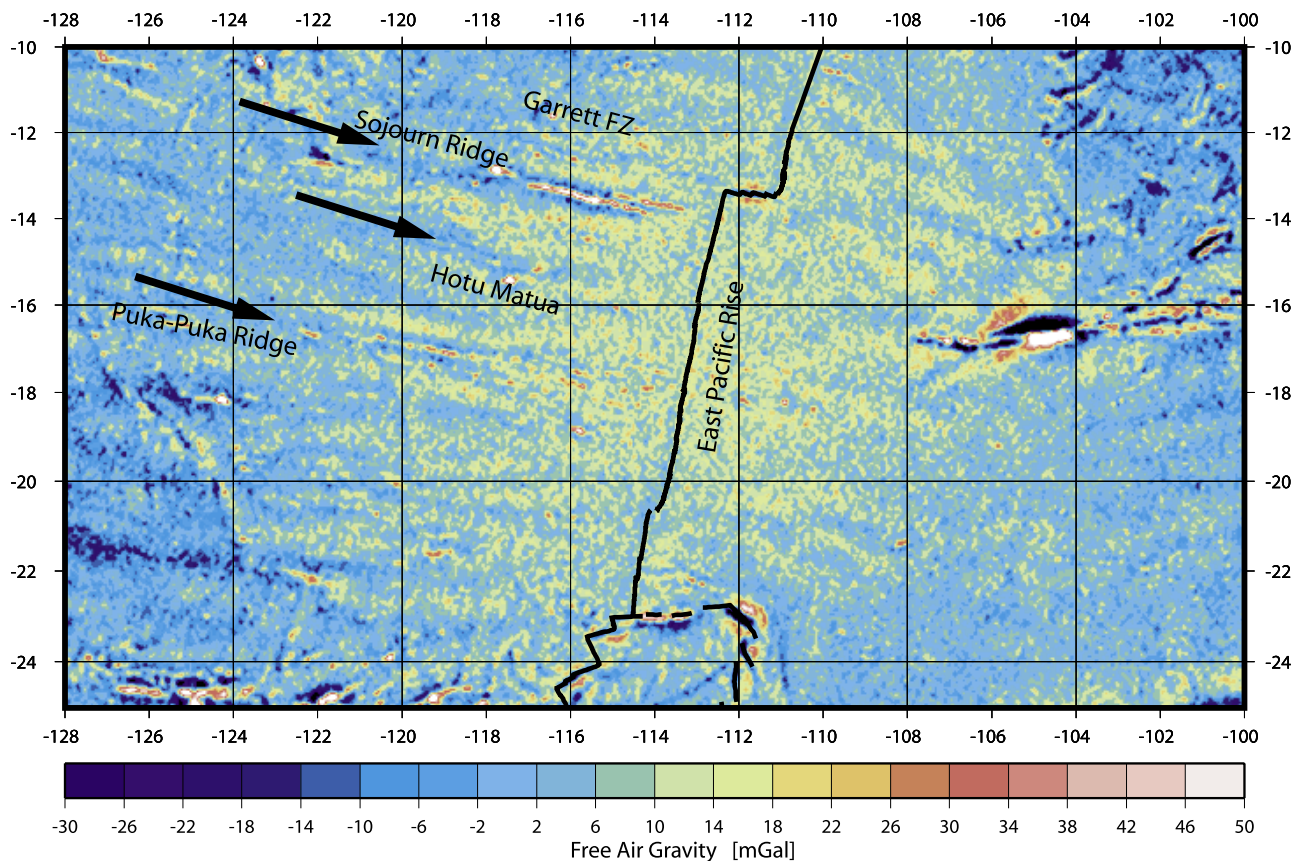


Figure 1. Satellite free-air gravity anomaly of the south central Pacific Ocean [Sandwell and Smith, 1997, v. 11.2]. Superimposed on the broad gravity high associated with the EPR are gravity lineaments that are approximately perpendicular to the spreading center in the direction of absolute plate motion of the Pacific plate. Note that the lineaments are absent near the EPR. Bold lines indicate plate boundaries. Arrows in the direction of Pacific plate motion indicate gravity lows associated with intraplate volcanic ridges. The major bathymetric features in the region are labeled.

relative to the underlying deeper mantle [Haxby and Weissel, 1986; Buck and Parmentier, 1986], but a variety of other mechanisms have since been suggested.

[3] Models explaining the existence of the gravity lineaments and the associated volcanic ridges can be grouped into two categories: those invoking dominantly lithospheric processes or those requiring active asthenospheric processes (Figure 2). In the lithospheric models, diffuse extension [Winterer and Sandwell, 1987; Sandwell et al., 1995] or bending and cracking of the lithosphere by thermal stresses [Gans et al., 2003; Sandwell and Fialko, 2004] produce the observed free-air gravity anomalies through topography created by thinning the crust or by flexure of the plate. The intraplate volcanism in these lithospheric models is produced by cracks tapping a reservoir of preexisting asthenospheric melt. Alternatively, asthenospheric models require some dynamic mantle process such as small-scale convection [Haxby and Weissel, 1986; Buck and Parmentier, 1986; Wessel et al., 1996; Barnouin-Jha and Parmentier, 1997; Marquart, 2001; Korenaga and Jordan, 2004], migrating minihot spots [Fleitout and Moriceau, 1992; Yamaji, 1992], or asthenospheric return flow [Conder et al., 2002; Weeraratne et al., 2003b] that organizes density anomalies beneath the lithosphere into the observed pattern of the

gravity anomalies and produces the volcanism through decompression melting.

[4] There are distinct differences in the predicted topography and density patterns for the different models. To clarify these patterns, in this paper, we subtract the topography and gravity effects of surface volcanic loading and the resulting flexure, which should be functions only of the distribution of the load and the flexural rigidity of the plate, not the mechanism of origin. The residual topography and residual mantle Bouguer gravity anomalies should directly reflect the underlying process. The thermoelastic cracking model (Figure 2a) predicts a residual topographic low beneath the volcanic ridges, but no Bouguer anomaly, because the plate is simply flexed downward with no change in density structure. The lithospheric stretching or boudinage model (Figure 2b) predicts a residual topographic low and a positive residual mantle Bouguer anomaly because the crust is thinned. Both the small-scale convection model (Figure 2c) and the channelized return flow model (Figure 2d) predict residual topographic highs and negative Bouguer anomalies because they assume low densities in the asthenosphere beneath the ridges.

[5] Successful testing of these models has been hampered because the remoteness of this part of the Pacific has led to

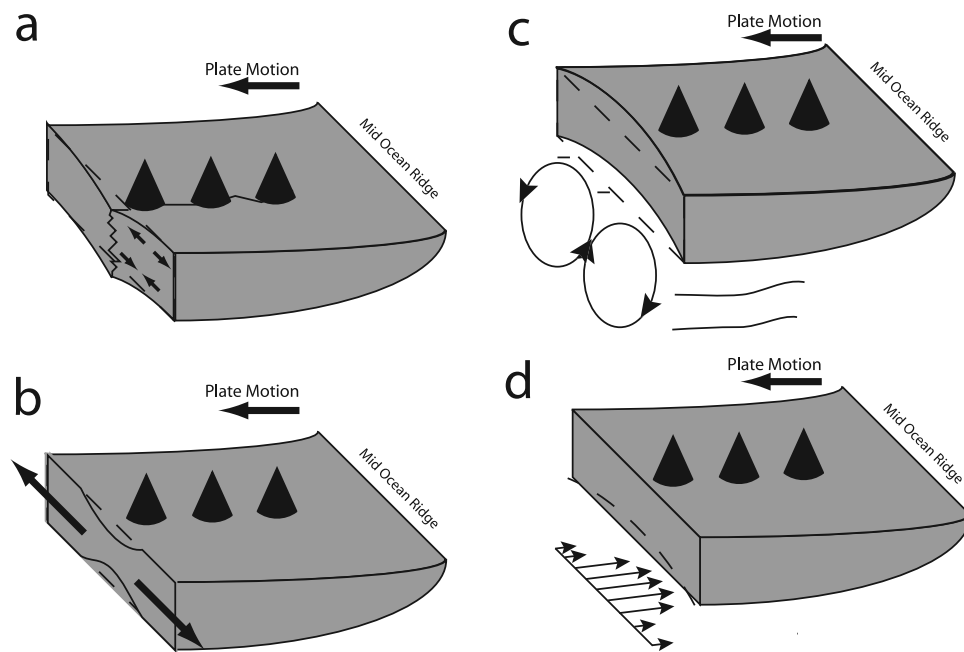


Figure 2. Schematic diagrams of proposed models of formation of the gravity lineaments, including the relationship to volcanic chains and underlying dynamic topography. (a) The thermoelastic cracking model predicts a topographic low beneath the volcanic edifices, with a corresponding free-air gravity low. We do not expect residual mantle Bouguer anomalies (rMBA) associated with this model because the volcanism is produced by tapping ambient asthenospheric melt with no alteration of lithospheric structure. (b) The lithospheric boudinage model predicts a topography low beneath the volcanic edifices if the isostatic effect of thinning of the crust is greater than the effect of thinning the thermal lithosphere. If this is true, there should be an rMBA high because the thinned crust is shallower than the thinned mantle lithosphere. (c) Small-scale convection predicts a topography high over the upwelling limbs of the convection cells beneath the volcanic edifices on young seafloor and little or no topography when the characteristic wavelength of flexure becomes greater than the wavelength of convection. On young seafloor, the free-air gravity will be dominated by the surface topography high while on stronger lithosphere the free-air anomaly should be dominated by the density anomalies associated with convection at depth. We also expect to see a negative rMBA associated with the upwelling. (d) Channelized return flow predicts a topographic high if the flowing mantle is hotter and less dense than adjacent asthenosphere and if the plate is flexible enough to respond to the subsurface load. There should be a negative rMBA associated with any low-density anomaly in the asthenosphere.

a paucity of bathymetric data. Previous work has been limited mostly to interpreting the regional satellite free-air gravity or geoid anomalies. Most investigators have assumed that gravity lows coincide with topographic lows, but, in fact, even this basic correlation has not been established at the relevant wavelengths. In the best existing study of the relationship between bathymetry and free-air anomalies in the Central Pacific, the coherence between topography and gravity is essentially zero at wavelengths of 200 km [McAdoo and Sandwell, 1989]. A problem with the study that may have led to the low coherence is the lack of two-dimensionality in features that were mapped using long, isolated profiles. One of the profiles used, for example, crosses the gap between the Sojourn Ridge and the large Southern Cross Seamount (see arrow, Figure 3); so that this spot appeared to be an independent topographic and gravity low even though it is a flexural low caused by the large, adjacent topographic loads that were not recognized. More complete bathymetric coverage is essential for understanding the origin of the gravity lineaments.

[6] The observation that the intraplate volcanic ridges lie preferentially in the troughs of the gravity lineaments [Sandwell and Fialko, 2004] provides an example of the ambiguity in interpretation that arises due to the lack of bathymetric coverage. Sandwell and Fialko's interpretation of this observation is that the ridges lie in preexisting topographic lows produced by the downward bending moment associated with thermal cooling of the lithosphere (Figure 2a). The topographic lows created in this way are uncompensated by high-density material at depth and thus generate significant negative free-air anomalies. Alternatively, flexural troughs created by the load of the volcanic ridges themselves are also uncompensated and would create flanking gravity lows, thus the association of a gravity trough with an intraplate ridge does not necessarily indicate that the ridge formed in a trough that would have existed without the ridge. Both the Sojourn Ridge and some of the most massive and linear parts of the Puka Puka ridge are flanked by some of the strongest negative free-air anomalies, suggesting a flexural influence. These lows are in turn flanked by broader gravity highs that stand out above the

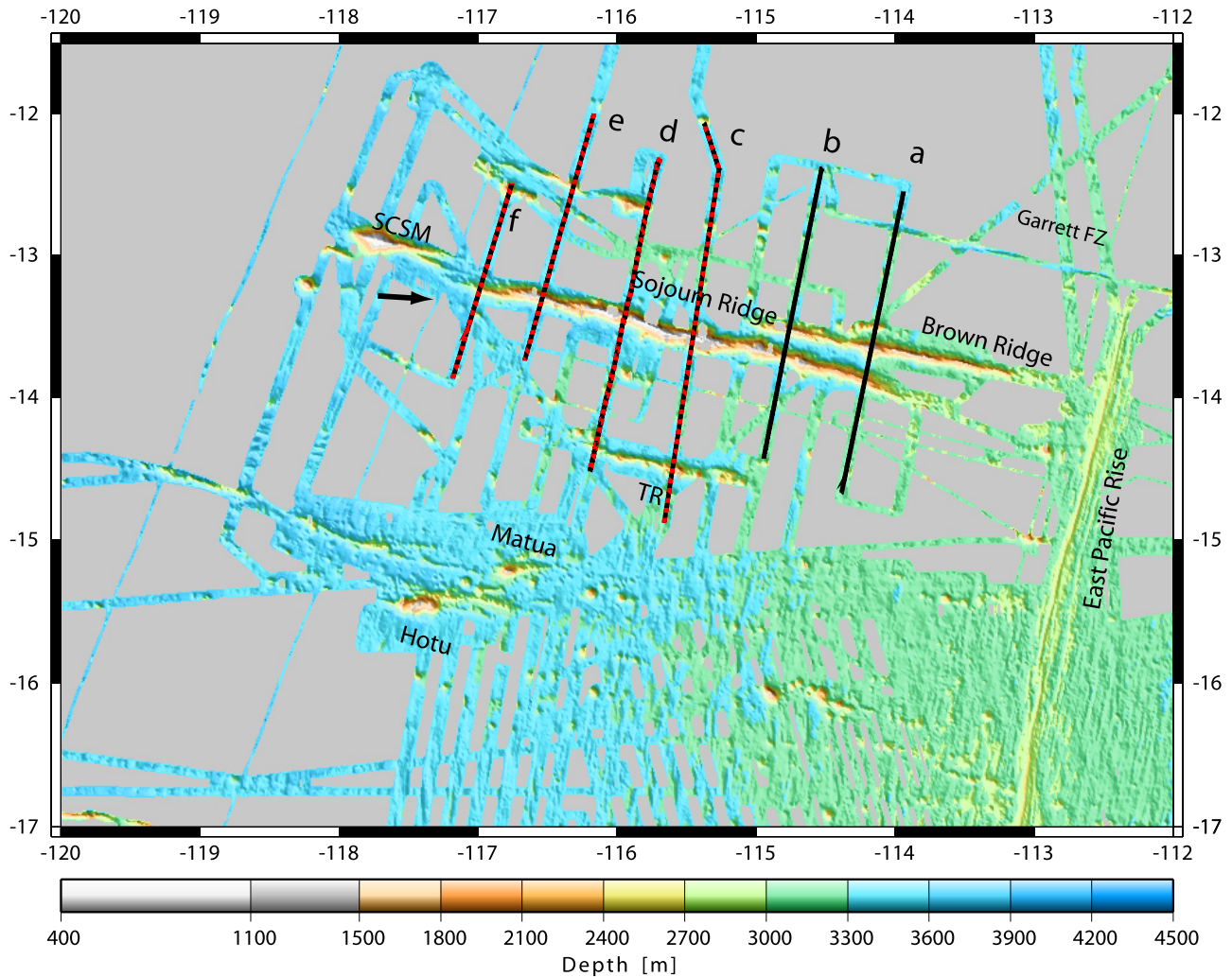


Figure 3. Bathymetry of the GLIMPSE study region illuminated from the southwest. Bathymetric surveying preferentially mapped the volcanic edifices in the region, with 49% coverage of the region. Black lines indicate the location of the profiles a–f across the Sojourn Ridge shown in Figure 7, while superimposed red dashed lines indicate the transects stacked for the 2-D gravity modeling shown in Figure 12. The major edifices and tectonic features in the region are labeled (SCSM indicates Southern Cross seamount, TR indicates Thanksgiving ridge). Arrow indicates where the track line in the *McAdoo and Sandwell* [1989] study crossed the Sojourn ridge system.

background level of free-air anomalies (Figure 1). The pattern resembles the pattern of the Hawaiian hot spot chain on a much smaller scale, where a volcanic chain with flexural moats sits atop a broad swell. The Hawaiian swell may be created by anomalously hot or depleted asthenosphere, and the same may be true of the highs flanking the Sojourn and Puka Puka ridges. *Sandwell and Fialko* [2004] showed that when low-pass filtered, the free-air anomalies at the crests of some of the ridges are negative, indicating that the anomalies are more negative than can be expected from flexure due to surface loading alone.

[7] The goal of this paper is to use the relationships between gravity and topography observed in the Gravity Lineations Intraplate Melting Petrologic and Seismic Expedition (GLIMPSE) Experiment to evaluate the hypotheses proposed for the origin of the gravity lineaments. GLIMPSE focused on two ridge systems that coincide with the beginning of well-developed troughs in the previously

recognized pattern of gravity lineaments: the Sojourn Ridge system, which also includes the Brown ridge and the Southern Cross Seamount, and the Hotu Matua volcanic complex (Figure 3).

2. Data Processing

[8] The studies presented here used shipboard bathymetry, shipboard gravity data and the free-air gravity anomaly derived from satellite altimetry [*Sandwell and Smith, 1997*]. The bathymetry of the GLIMPSE study area is a compilation of the Sojourn 1, Sojourn 9, Gloria 2, Gloria 3, Gloria 8, Boomerang 1, Westward 1, Westward 4, Rapa 2, Cook 16, Vancouver 4, RC2608, and HS145-1 cruises, plus some additional data from the RIDGE cruise multibeam synthesis (see *Scheirer et al. [1996]* for a prior version of this compilation). The ship tracks for the Cook and Vancouver cruises were designed to survey the major ridges and seamounts in

the northern GLIMPSE study area, and the southern third of the study area coincides with the northern Mantle Electromagnetic and Tomography (MELT) area [Forsyth *et al.*, 1998; Scheirer *et al.*, 1998]. A SeaBeam2000 multibeam sonar system on the R/V *Melville* collected the bathymetry data for the Sojourn, Gloria, Boomerang, Westward, Rapa, Cook and Vancouver cruises. The RC2608 and RIDGE data used SeaBeam and the HS145-1 data used a Hydrosweep system [Grevenmeyer *et al.*, 2002]. The SeaBeam2000 data cruises were processed using a despiking algorithm developed by Forsyth and Scheirer and then hand edited using MB System software to remove artifacts due primarily to sea state-dependent noise caused by bubbles entrained beneath the ship's hull. The compiled, processed data from all of the individual cruises were averaged and gridded using Generic Mapping Tools (GMT) software [Wessel and Smith, 1991] on 200 m and 1000 m grids. Approximately 258,000 km² surface area was mapped in the GLIMPSE study area corresponding to 49% coverage of the area in Figure 3.

[9] To aid in the interpolation of the bathymetry data and the analysis of the effects of surface loading, we isolated seamounts and ridges from the background topography using the median filter approach of Shen *et al.* [1993] (Figure 4a). In this approach, a point is identified as being anomalously shallow by comparing its depth to the median depth in a long, thin rectangular region aligned perpendicular to the spreading direction and centered on the point. A nearest neighbor interpolation scheme was used to fill in empty, unmapped grid points for the isolated seamounts while the relatively smooth residual, background topography was interpolated using the cubic spline surface routine in GMT. Adding these two fields together gives a complete estimated map of bathymetry without distortions from extrapolating seamount bathymetry into unmapped areas that are probably dominated by abyssal hill topography.

[10] After interpolation, both the residual seafloor topography and the satellite free-air gravity anomaly were detrended to remove the dominant gradients due to subsidence of the seafloor with age. The detrending of the data was intended to highlight the gravity lineaments and seamounts, which run parallel to the age gradient of the seafloor. We chose to remove the trend as a function of distance away from the EPR with a simple polynomial function of the form:

$$y(x) = ax + b\sqrt{x} + c \quad (1)$$

where y is the seafloor depth, x is the distance from the ridge axis, and a , b , and c are model coefficients. The results of the filtering, interpolating and detrending are shown in Figure 4b. The axial high of the East Pacific Rise remains in this filtered version, but most other features are ridges, seamounts, and their flanking lows that are parallel to the spreading direction. The \sqrt{x} term is chosen to represent the subsidence which is approximately proportional to square root of age, or distance from the ridge with the nearly constant spreading rate, and the linear term removes any regional trends, such as those associated with temperature gradients or return flow that have been proposed for this area [e.g., Cochran, 1986; Toomey *et al.*, 2002]. Shipboard gravity data were collected on the Cook 16 leg of the R/V

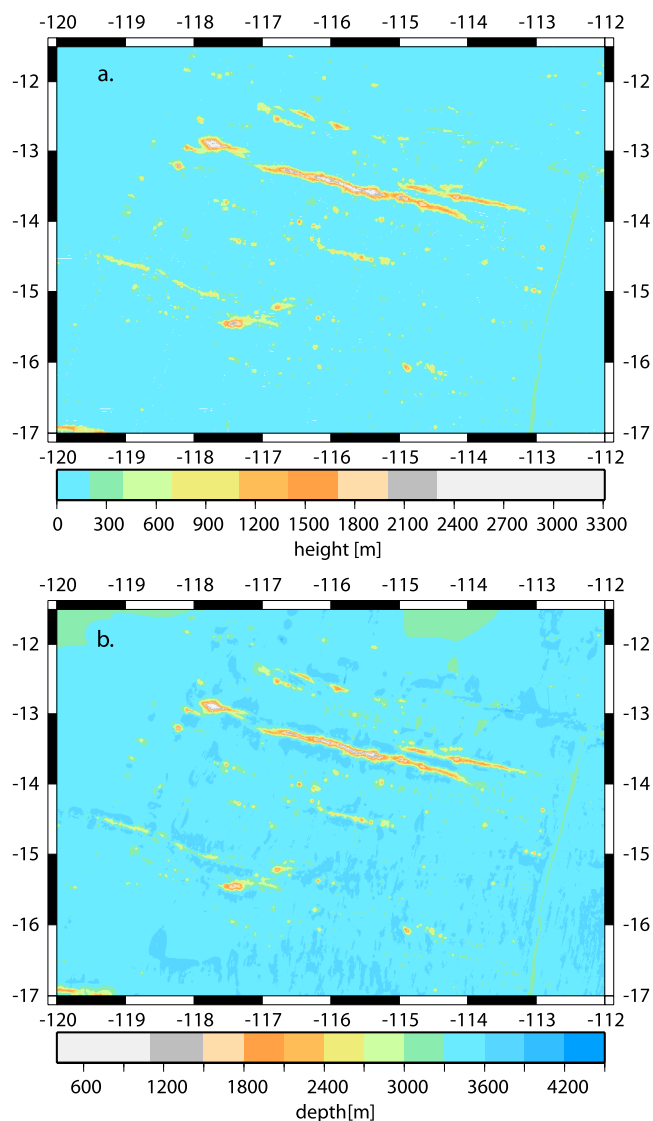


Figure 4. Isolated seamounts and interpolated detrended bathymetry. (a) The seamounts and ridges have been isolated with a median filter and interpolated to fill in any gaps in coverage. (b) Interpolated bathymetry after removal of the deepening of the seafloor with increasing age; the background depth has been arbitrarily set to 3500 m. This map is constructed by adding Figure 4a to an interpolation of the background topography after removal of seamount edifices and age trend.

Melville, and were added to an existing data set from prior cruises in the GLIMPSE study area [Scheirer *et al.*, 1998]. The data were collected every second, smoothed, Eotvos corrected, and a reference Earth gravity field removed to yield a free-air anomaly at a 1-min interval. Although track line gravity coverage is sparse overall, it is sufficient over some of the edifices and the surrounding moats to provide an accurate picture of the free-air anomaly in those regions. Crossover errors between track lines were minimal, and systematic offsets between cruises were corrected with a DC shift where necessary. In the regions around Hotu and Matua seamounts, for example, the residual RMS crossover

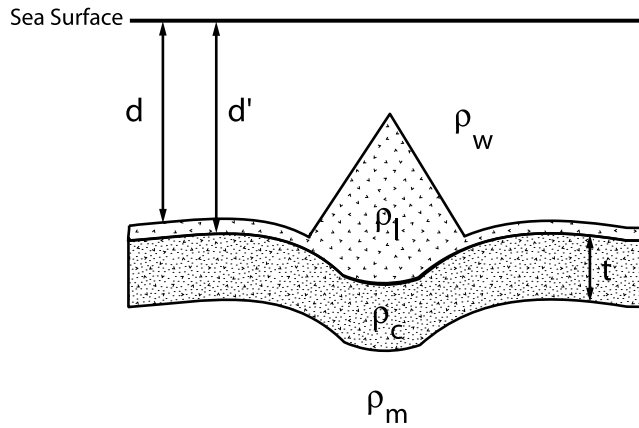


Figure 5. Simple flexure model with surface loading only. There are three density interfaces, the water-load boundary, load-preexisting crust boundary, and the crust-mantle boundary. In this model, the infill is assumed to be water. The variables shown in the diagram correspond to the variables in equations (2), (3), and (4).

errors among all cruises were 1.4 and 2.3 mGal (1 mGal = 10 g.u.), respectively after DC shift corrections, within typical measurement uncertainty of a shipboard gravimeter.

[11] We did not merge the shipboard and satellite gravity observations because the shipboard data were too sparse and because the satellite gravity was significantly lower resolution than shipboard data where they coincided. As described below, we used the shipboard data for estimating the density and flexural characteristics of the individual features that had sufficient coverage, and we used the satellite data, provided on 2-min grids [Sandwell and Smith, version 11.2, <http://topex.ucsd.edu>], for studying the regional pattern of gravity anomalies. To compare the anomalies created by the seafloor topography and other density interfaces to the observed satellite gravity, we calculated the attraction using the interpolated, 1-km bathymetry grid and a Fourier transform technique [Parker, 1973], applied a low-pass filter that mimicked the transition from high to low coherence between satellite altimeter and shipboard gravity data [Yale et al., 1995; Sandwell and Smith, 2005], and then regridded the theoretical gravity anomalies onto 2-min grids.

3. Effective Elastic Thickness and Density of Seamounts and Ridges

[12] To evaluate the contribution of flexure of the lithosphere to the observed free-air gravity lows in the GLIMPSE study region, we model the gravitational effects of loading the volcanoes and ridges onto a thin elastic plate. This, in turn, requires estimates of the bulk density of the seamount loads and the effective elastic thickness of the lithosphere. To obtain initial estimates, we searched over a range of possible seamount densities from 1500 to 3200 kg m⁻³ and effective elastic thickness T from 0 km to 20 km to find the best fit to the gravity data, assuming flexure of a uniform thickness plate with surface loading only. We assume the surface load with density ρ_l is

emplaced on a crust of constant initial thickness t (Figure 5) and uniform density ρ_c . We neglect any increase in density with depth because the predicted gravity anomaly for a uniform density is indistinguishable from that of a stratified crust. This model assumes that the infill of flexure is seawater because high-resolution, single-channel reflection profiles showed that sediment ponds within the topographic lows that flank some of the largest seamounts and ridges are a maximum of 50 to 100 m thicker than sediments in the surrounding regions, which is much smaller than the total deflection, leaving a largely water-filled moat. Abyssal hill topography is identifiable close to the Sojourn ridge and south of the Hotu seamount, indicating that the flexural moats have not been filled in with lava flows [Forsyth et al., 2006].

[13] Given an assumed elastic plate model, the deflection $y(x)$ due to surface loading can be predicted by a linear filter applied to the resulting surface topography $h(x)$. We perform this filtering in the wave number or spatial frequency domain so that

$$Y(k) = -H(k) \left[\frac{\rho_m - \rho_w}{\rho_l - \rho_w} \Phi(k) - 1 \right]^{-1} \quad (2)$$

$$\Phi(k) = \left[1 + \frac{Dk^4}{(\rho_m - \rho_w)g} \right]^{-1} \quad (3)$$

where $H(k)$ and $Y(k)$ are the Fourier transform of $h(x)$ and $y(x)$, k is wave number $2\pi/\lambda$, where λ is wavelength, D is the flexural rigidity defined as $ET^3/12(1 - \nu^2)$ where E is Young's modulus T is effective elastic thickness and ν is Poisson's ratio, g is the acceleration of gravity, ρ is the density of the load (l), mantle (m), crust (c) or water (w), and Φ is the flexural filter [Watts, 2001].

[14] The predicted FAA gravity anomaly is given by

$$\Delta g(k) = 2\pi G \left[(\rho_l - \rho_w) \exp(-kd) \sum_n \frac{k^{n-1}}{n!} \mathfrak{F}\{h^n(x)\} + [(\rho_c - \rho_l) + (\rho_m - \rho_c) \exp(-kt)] \exp(-k(d')) Y(k) \right] \quad (4)$$

where $\Delta g(k)$ is the gravity anomaly in the wave number domain, G is the gravitational constant, d is the median water depth, d' is median depth to the base of the load, t is the average thickness of the crust before loading, \mathfrak{F} is the Fourier transform operator and [Watts, 2001; Parker, 1973]. The index n in the Taylor series for the attraction of the load ranged up to 4 when required by the height of the edifice, but only the first-order term was required for the interface between load and preexisting crust or for the crust-mantle interface. We assumed Young's modulus E is 1×10^{11} N m⁻², Poisson's ratio ν is 0.25, ρ_w is 1030 kg m⁻³, ρ_c is 2800 kg m⁻³, ρ_m is 3300 kg m⁻³, d' is 4.0 km, and t is 6 km. The Fourier transforms are two-dimensional for mapped features and one-dimensional for profiles.

[15] For each major bathymetric feature, including Hotu, Matua, Southern Cross Seamount (SCSM), Sojourn Ridge and Brown Ridge, we defined a subregion that encompassed the entire edifice and as much of the surrounding area as

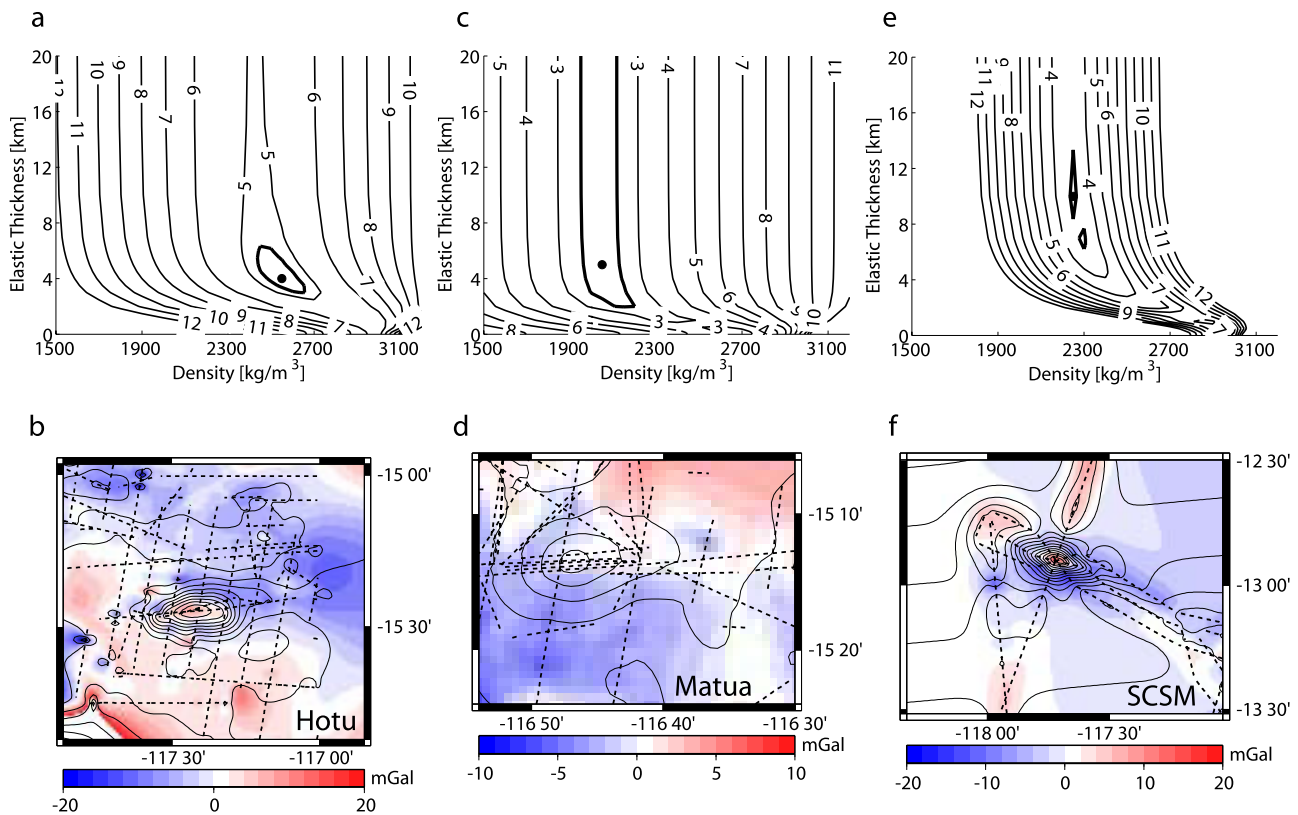


Figure 6. Estimates of density and effective elastic thickness for seamounts. (a, c, e) The plots show contours of equal misfit of gravity anomalies in least squares sense with the bold line outlining the 95% confidence region. The black dot is the best fitting model. (b, d, f) Plots of Hotu (Figures 6a and 6b), Matua (Figures 6c and 6d), and SCSM (Figures 6e and 6f) are the residual gravity of the best fitting model in the red-blue scale and the original free-air gravity anomalies shown at 5 mGal contour intervals. The dashed black lines indicate the shipboard gravity measurement locations.

possible without contamination from other seamounts. We chose the shipboard gravity because it has finer resolution than the satellite gravity with lower noise levels at short wavelengths and greater accuracy over the peaks of large seamounts [Maia, 2006]. Coherence of shipboard gravity data with bathymetry extends to wavelengths of 12–13 km, while resolution of even the latest satellite gravity (V15 of Sandwell and Smith, not available at the time of submission of this paper) is limited to wavelengths of about 15 km [Neumann et al., 1993; Smith and Sandwell, 1997; Sandwell and Smith, 2005; Maia, 2006]. Crossover errors of the shipboard data were 1.4 to 2.3 mGal, representing a reduction in variance on the order of 50% from the typical 2.7 to 3.3 mGal RMS disagreement between shipboard profiles and the satellite-derived gravity [Maia, 2006]. In the case of the Sojourn and Brown ridges, we chose single track lines for analysis because shipboard gravity exists only for a few crosslines and bathymetric surveying of the regions flanking the ridges is limited. Single track lines are appropriate for ridges that approximate two-dimensional (2-D) features, i.e., extending infinitely perpendicular to the track line. If the bathymetry was incomplete, it was interpolated using GMT's splines under tension scheme with a tension of 1 [Wessel and Smith, 1991]. The predicted gravity for each combination of seamount density and elastic

thickness was calculated from the topography of the subregion, sampled along the track lines (shown in Figure 6), and subtracted from the observed shipboard gravity data along those tracks. The variance of the gravity residual was calculated and tabulated for each model. In the case of the shallow Southern Cross Seamount, we included the higher-order Taylor series terms in the calculation of the predicted gravity to remove the systematic error over the shallow peak of the seamount due to significant contributions from the nonlinear terms. Therefore, in this case the summation index from equation (4) was set to 4. After tabulating the variance of each model in the grid search, we needed to determine the number of independent gravity observations to calculate confidence limits on the best fit load density and effective elastic thickness values. Track line gravity anomalies over seafloor away from seamounts were analyzed to estimate noise in the gravity signature. The free-air gravity observations from these track lines were autocorrelated, and the first zero crossing of the correlograms was used to determine the distance between independent measurements of gravity. In all cases, the average distance per independent measurement was thus determined to be 8 km. Hence we divided each of the edifice subregions into 8 km by 8 km cells, and assigned the number of cells containing gravity data to equal the number of independent measurements for

Table 1. Effective Elastic Thickness and Seamount Density Estimates

Edifice Name	T, km	Load Density, kg m ⁻³	Lithospheric Age, Ma	Figures	Estimate Type
Hotu	4	2550	6.2	6a and 6b	grid
Matua	5	2050	6	6c and 6d	grid
Southern Cross	10	2250	8.2	6e and 6f	grid
Sojourn 114°13'W	5	2400	2.6	7a	profile
Sojourn 114°48'W	3	2300	3.6	7b	profile
Sojourn 115°27'W	3	2500	4.6	7c	profile
Sojourn 115°57'W	2	2600	5.6	7d	profile
Sojourn 116°32'W	4	2400	6.6	7e	profile
Sojourn 116°59'W	3	2600	7.8	7f	profile

the subregion inversion. The approximate 95% confidence regions were determined by finding points that satisfy:

$$S(\rho_l, T) = \hat{S}(\rho_l, T) \left[1 + \frac{p}{n-p} F(p, n-p, 1-q) \right] \quad (5)$$

where S is the sum of the squares of the misfits at grid search point ρ_l and T , and \hat{S} is the minimum misfit for the sum of the squares of the misfits for the best fitting model [Draper and Smith, 1998]. The function F is the F statistic with a $(1 - q)$ confidence level, 95%, and with p and $n - p$ degrees of freedom, where p is the number of parameters and n is the number of independent observations.

[16] The grid search revealed estimates for effective elastic thickness among the study areas ranging from 2 to 10 km with an average of ~ 4 km. Southern Cross Seamount appears to have formed on more rigid lithosphere (10 km) than the Sojourn Ridge, while the rest of the seamounts in the region appear to have formed on 2- to 5-km-thick elastic lithosphere. The seamount load densities ranged from 2050 to 2600 kg m⁻³ with an average of 2400 kg m⁻³. Matua and Southern Cross seamounts have particularly low values of 2050 and 2250 kg m⁻³, respectively. The results are given in Table 1, and examples of the original free-air anomalies and remaining residuals are shown in Figure 6 (2-D inversions). Figure 7 (1-D inversions) compares the original and predicted FAA. Residual anomalies have no correlation with the topography and appear to be continuations of the regional gravity anomalies. The superposition of the regional gravity anomalies on the free-air anomaly of the local edifice and the lack of visible moats surrounding the Southern Cross and Matua seamounts yield well-constrained lower bounds on thickness, but poorly constrained upper bounds (Figures 6c and 6e). In addition, transects b and f (Figure 7) exhibit large ranges in effective elastic thickness and load density in their 95% confidence regions. The poor constraint on the model parameters for these two transects is due to a relatively poor fit to the observed gravity caused by their location near the ends of the Brown and Sojourn ridges and the consequent breakdown in the assumption of two-dimensionality.

[17] Although the total range of effective elastic thicknesses is roughly what is expected for seafloor of age 3 to 9 Ma if the thickness is controlled by the 450°C isotherm in the cooling plate [Watts, 1978; Calmant and Cazenave, 1987], the distribution of thicknesses through the study area does not follow the expected pattern. Except for the Southern Cross Seamount, there is no significant variation

of T with age of the seafloor. Most of the values cluster in the lower part of the range, and thus most of the values are lower than predicted for the thermal model. Goodwillie [1995] also found apparent elastic thicknesses for the Puka Puka ridges of a few kilometers on even older seafloor expected to have elastic thicknesses up to 17 km. There may be several factors responsible for the low values and lack of increase with age. Previous studies of seamounts have reported that the elastic thickness of the lithosphere in the South Pacific is thinner than that of seafloor of the same age in other oceans [Calmant and Cazenave, 1986; Wessel, 1992; Lyons et al., 2000], possibly due to anomalous heating of the lithosphere in the superswell region [McNutt and Judge, 1990]. Other studies dispute the low estimates of rigidity in the area, finding results concordant with other oceans [Filmer et al., 1993; Grevemeyer et al., 2001]. In the GLIMPSE and MELT study areas, the seafloor subsides anomalously slowly with increasing age [Cochran, 1986], perhaps indicating slower thickening of the lithosphere caused by asthenospheric transport of anomalously hot mantle from the superswell in the west to the East Pacific Rise [Phipps Morgan et al., 1995; Toomey et al., 2002; Conder et al., 2002; Gaboret et al., 2003]. Some of the seamounts could have formed nearer the EPR when the underlying lithosphere was younger and weaker. Hotu seamount, for example, has no recent lava flows and appears older than other seamounts in the area. In contrast, microearthquake activity, recent lava flows, and radiometric dating all indicate that Matua is still forming, and radiometric dates indicate that the Sojourn Ridge formed within the last 1–2 Myr [Forsyth et al., 2006]; it is clear that those features were not emplaced near the EPR. The lithosphere could have been thinned or weakened during the emplacement of the volcanic edifices, as suggested by the anomalously low shear velocities in the uppermost mantle beneath the Sojourn and Brown ridges [Weeraratne et al., 2003a]. Finally, estimates of flexural rigidity based on gravity and topography alone depend on the model of isostatic compensation. There are tradeoffs between elastic thickness, density of infill, load density and depth of compensation, and if there is subsurface loading in addition to the surface load of the seamount itself, the estimate of elastic thickness based on surface loading may be biased [Forsyth, 1985; Grevemeyer and Flueh, 2000; Grevemeyer et al., 2001; Minshull and Charvis, 2001].

[18] Densities of seamounts and ridges in the GLIMPSE area (Table 1) are lower than typically reported bulk densities of 2600–2800 kg m⁻³ of other seamounts [e.g.,

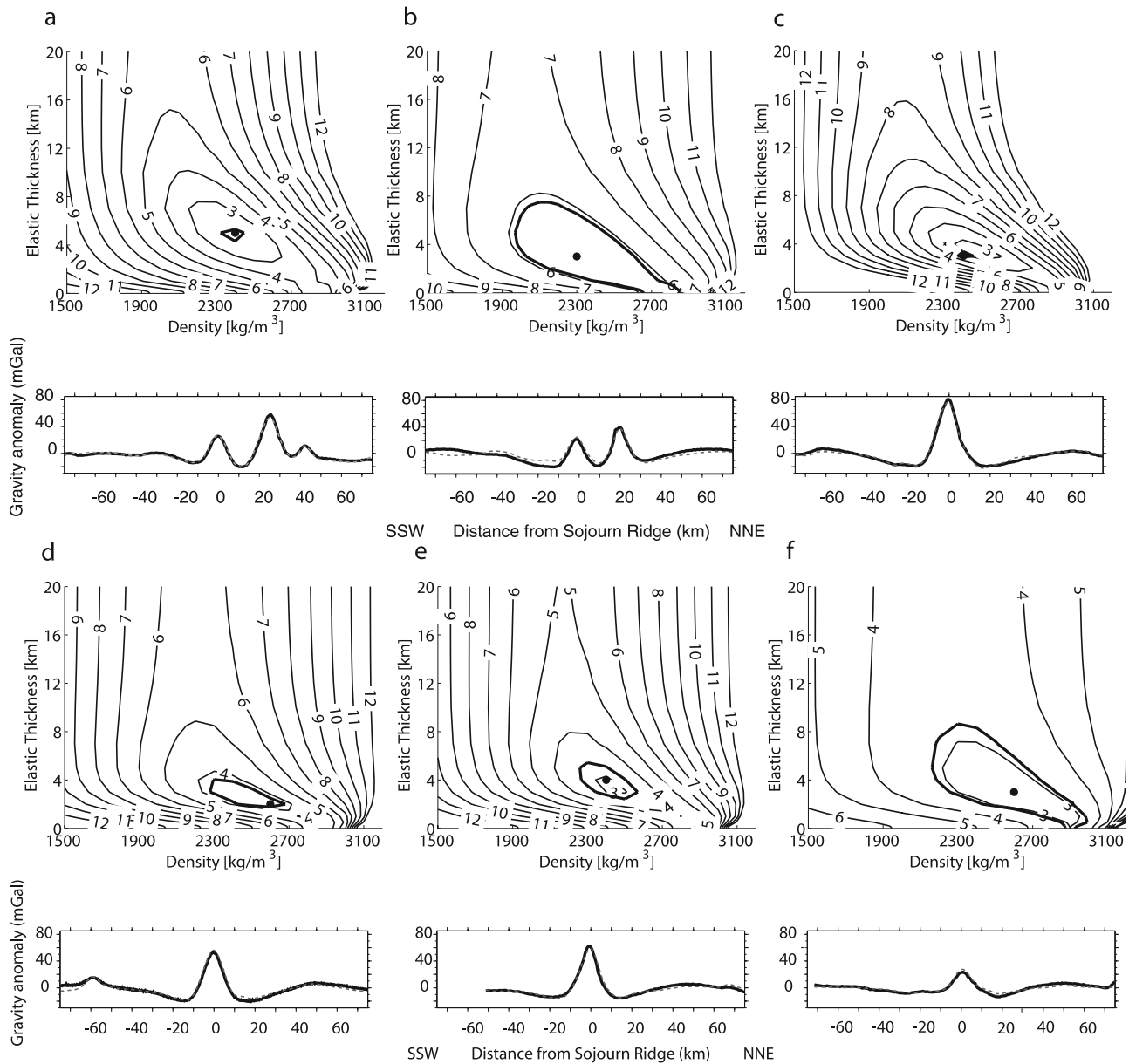


Figure 7. Estimates of density and effective elastic thickness for profiles crossing the Sojourn ridge. Figures 7a–7f are for profiles a–f shown in Figure 3. (top) Contours are of equal misfit, with the bold line indicating the 95% confidence region and the black dot indicating the best fitting model. (bottom) Contours are the observed free-air gravity anomaly in black and the free-air anomaly predicted by the best fitting model in dashed grey lines.

Hyndman *et al.*, 1979; Ishihara, 1987; Lyons *et al.*, 2000]. Southern Cross seamount and Matua are particularly low. There are two possible explanations for the low-density observations: either the seamounts are constructed of low-density, highly porous volcanic material or subsurface loading is masking the true density of the seamounts in the inversion that assumes only top loading. Both ideas are plausible. Highly silicic (> 55 wt%) volatile-rich, vesicular rocks have been dredged near the EPR [Stoffers *et al.*, 2002]; dredging of the Matua seamount produced some highly vesicular basalts, and one rock sample had a bulk composition of 70 wt% SiO_2 , although most samples recovered from Matua and other features in the GLIMPSE area

were nonvesicular, basaltic tubes, pillows, or flows. Jasper seamount off the coast of California has an apparent density of $\sim 2300 \text{ kg m}^{-3}$ [Harrison and Brisbin, 1959; Hammer *et al.*, 1991], which seismic tomography shows is probably caused by a thick, porous, low-velocity extrusive layer [Hammer *et al.*, 1994]. In addition, Minshull and Charvis [2001] used a method similar to this study to reexamine the elastic thickness and load density of the Marquesas and found a load density of 2550 kg m^{-3} with an elastic thickness consistent with the estimate determined from seismic refraction. The porous nature of basalts and extrusive formations could well explain the $\sim 2500 \text{ kg m}^{-3}$

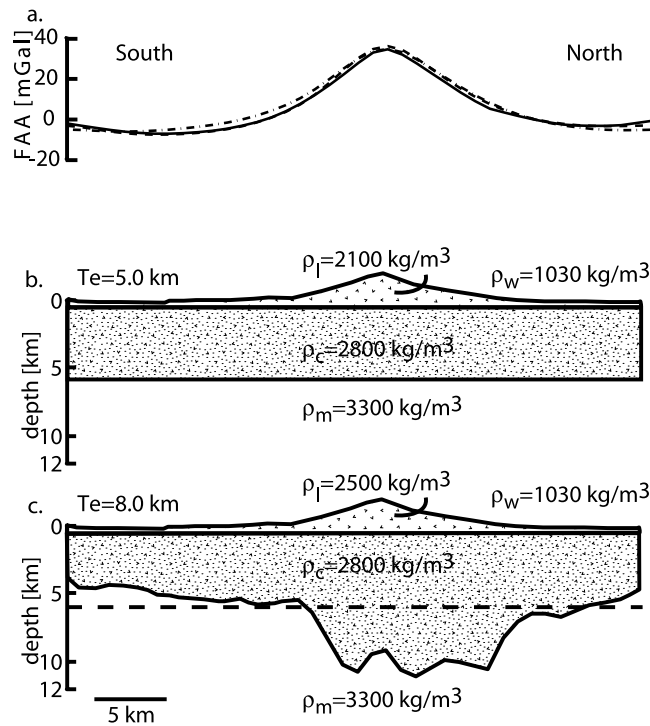


Figure 8. Alternative models of density structure beneath Matua seamount, illustrated along a north-south profile through the center of the seamount. Models themselves are three dimensions. (a) Free-air anomaly. Solid line is observed, dotted dashed line is best prediction of flexural model with surface loading only ($T_e = 5 \text{ km}$), and dashed line is prediction of flexural model with surface and subsurface loading ($T_e = 8 \text{ km}$). For each model, surface topography is fit perfectly. (b) The density structure and the magnitudes of the surface topography, crustal thickness and resultant flexural topography. For a small seamount like Matua, the amount of flexure is small with $T_e = 5 \text{ km}$. (c) The surface and subsurface topography and crustal thickness. The subsurface load shown was calculated as a perturbation to Moho topography at 6 km depth for a 8 km thick elastic plate. The subsurface load required is roughly cylindrical, 5 km in height and 15 km in diameter displaced slightly to the north. The fit to the observed gravity is very good and demonstrates that this model can also successfully explain the topography and gravity of Matua with a more reasonable density structure and greater elastic thickness.

densities typical of most of our estimates, but probably not the very low values observed for Matua and SCSM.

[19] We prefer the alternative explanation that the anomalously low apparent seamount densities are caused by neglected subsurface loading. The gravity and topography of Matua can be explained equally well with a more reasonable seamount load density of 2500 kg m^{-3} , if near-Moho subsurface loads are introduced and the flexural rigidity is equal to or greater than the rigidity estimated for surface loading. The required subsurface load is roughly cylindrical, displaced somewhat to the north of the peak of Matua, and about 15 km in diameter (Figure 8). If the load is in the form of crustal underplating with a density contrast

of -500 kg m^{-3} with respect to surrounding mantle, then it is equivalent to a $\sim 4 \text{ km}$ increase in crustal thickness. The implication is that our estimates for elastic thickness and density are minimums and, in the case of Matua, an unreasonable minimum for density.

[20] The existence of underplating is strongly supported by seismic refraction/wide-angle reflection observations showing that Sojourn Ridge is underlain by thickened crust over a region substantially wider than the edifice itself (R. C. Holmes et al., Crustal structure beneath gravity lineations in the GLIMPSE study area from seismic refraction data, submitted to *Journal of Geophysical Research*, 2006, hereinafter referred to as Holmes et al., submitted manuscript, 2006); the thicker crust thus could not have formed simply by downward flexure beneath the ridge. The absence of clear topographic moats around Matua and Southern Cross, in contrast to Hotu and Sojourn, suggests that these two seamounts have unusually large subsurface loads that buoy up the surrounding seafloor, hiding the flexure due to the seamounts themselves.

4. Regional Free-Air Anomalies

[21] Ultimately, we wish to investigate map view patterns of the gravity lineaments and not be restricted to scattered gravity track lines over the major edifices in the region. Because no gravity data was obtained on several cruises, bathymetric coverage is much more complete than ship-board gravity. To obtain uniform coverage for regional analysis, we use the interpolated, age-detrended bathymetry (Figure 4b) in conjunction with the age-detrended satellite, free-air gravity anomaly (Figure 9a).

[22] We want to estimate on a regional basis the maximum contribution to the free-air gravity anomaly of seamount loading and resultant flexure of the lithosphere. In other words, by varying elastic thickness and load density among other parameters can we completely explain the gravity lineaments with a simple flexural model? Using a damped, iterative least squared inversion and assuming surface loading only, we estimated the seamount density, effective elastic thickness, mantle density, and low-pass filter parameters that best matched the observed satellite free-air gravity anomaly in the region. The low-pass filter is needed to mimic the insensitivity of the satellite altimetry to short wavelengths and is parameterized by a 50% pass wave number and the width of the transition between no pass and 100% pass. The starting values for the model were 2600 kg m^{-3} for the seamount density, 5000 m for the effective elastic thickness, and 3300 kg m^{-3} for the mantle density. While we expected the elastic thickness of the plate to increase with age, our grid search inversions of individual areas did not indicate significant increase in elastic thickness in the region for the Sojourn Ridge or Hotu. Therefore, for simplicity, we model the effective elastic thickness as a constant throughout the region.

[23] The form of the iterative damped least squares inversion was that of *Tarantola and Valette* [1982]:

$$\hat{\mathbf{m}}_{l+1} = \mathbf{m}_l [\mathbf{G}_l^T \mathbf{C}_{mm}^{-1} \mathbf{G}_l + \mathbf{C}_{mm}^{-1}]^{-1} \cdot [\mathbf{G}_l^T \mathbf{C}_{mm}^{-1} \{\mathbf{d} - \mathbf{g}(\mathbf{m}_l)\} - \mathbf{C}_{mm}^{-1} (\mathbf{m}_l - \mathbf{m}_0)] \quad (6)$$

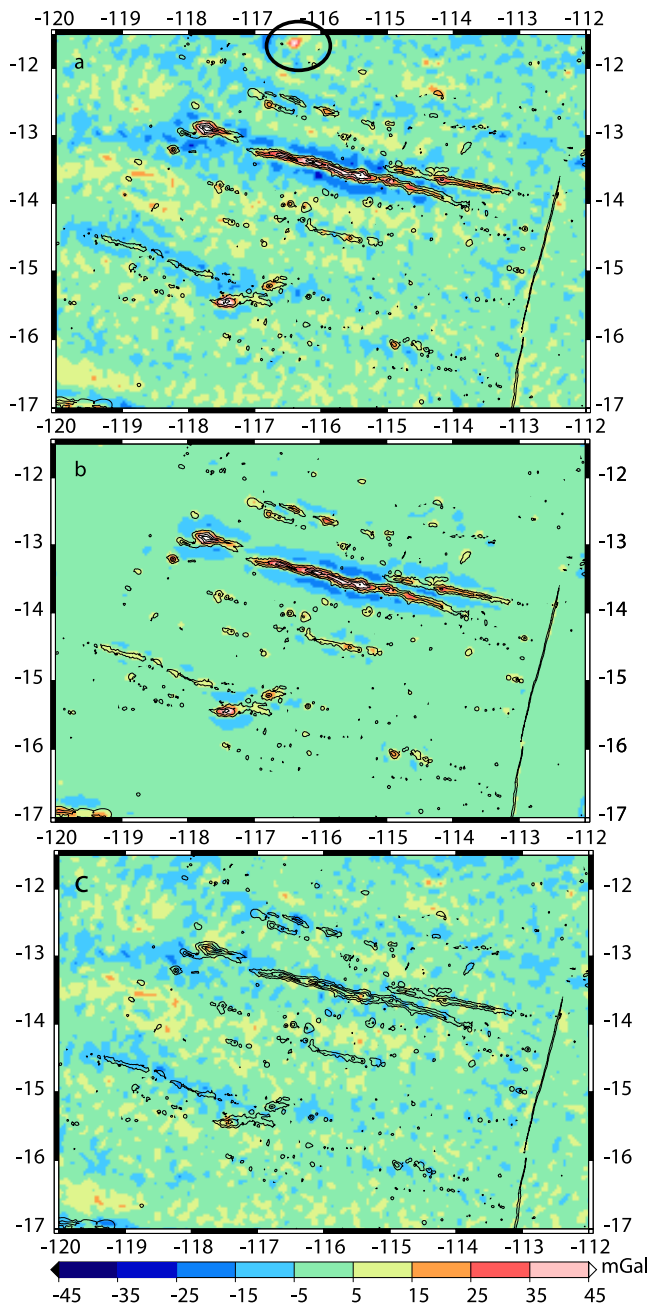


Figure 9. Modeling the free-air anomaly with surface topographic loading only. (a) Age-detrended free-air anomaly observed by satellite. (b) Predicted free-air anomaly with surface topographic loading based on mapped bathymetry and optimum estimates of load density ($\sim 2300 \text{ kg m}^{-3}$) and effective elastic thickness ($\sim 3 \text{ km}$). (c) Residual after subtracting Figure 9b from 9a. The circled region in the observed free-air anomaly was replaced with Gaussian noise for ease of convergence of the inversion because there was no bathymetry data for the feature. Black contours indicate the bathymetry contours at 800-m intervals showing the major bathymetric features in the region, using detrended bathymetry from Figure 4b. In the residual gravity the anomalies over the Sojourn Ridge and Hotu Matua have been reduced to near the regional noise levels; however, there persists a systematic gravity low oriented in the trend of APM in the data.

where \mathbf{m}_l is the model parameter vector of the l th iteration, \mathbf{G} is the matrix of partial derivatives of the predicted free-air anomalies at each point with respect to changes in the model parameters, \mathbf{C}_{nn} is the a priori data covariance matrix, \mathbf{C}_{mm} is the a priori model covariance matrix that introduces damping, \mathbf{d} is the satellite free-air gravity data vector and $\mathbf{g}(\mathbf{m}_l)$ is the l th forward model. We iterated until the change in the model parameters was less than one part in 10^{-6} . There was some nonlinearity in the model due to the low-pass filtering. To stabilize the nonlinear problem we introduce damping coefficients for the seamount density, mantle density, and elastic thickness corresponding to a priori model standard deviations of 500 kg m^{-3} , 500 kg m^{-3} , and 1000 m , respectively, to prevent physically unreasonable answers. Strong trade-offs between the filter center frequency and elastic thickness required us to damp the center wave number parameter with an a priori standard deviation of $1 \times 10^{-6} \text{ km}^{-1}$.

[24] The best fitting seamount density is $\sim 2300 \text{ kg m}^{-3}$, the elastic thickness is $\sim 3 \text{ km}$ and the mantle density is $\sim 3300 \text{ kg m}^{-3}$, roughly the same as averages derived earlier from the inversions for individual edifices. The effective elastic thickness is somewhat less than the average of the individual values obtained for Hotu, Matua and Sojourn, probably because we now include the Brown Ridge, which is currently forming on young seafloor, and smaller edifices like the Thanksgiving seamounts (Figure 3) that we believe formed near the East Pacific Rise and were carried to their current location by the movement of the Pacific plate [Forsyth *et al.*, 2006]. Thus, although the flexural rigidity of Sojourn shows little variation along its length, there does seem to be an increase in rigidity with age of the seafloor at the time of loading.

[25] The free-air residual of the best fitting inversion (Figure 9c) shows that the simple surface loading flexural model is capable of reducing the anomaly directly over the edifices to a approximately zero mean with laterally varying anomalies no larger than the scattered anomalies in the surrounding regions. Although the form of the predicted anomalies (Figure 9b) resembles the observed free-air anomalies around Sojourn, Southern Cross and Hotu (Figure 9a), clear negative residual anomalies remain in the area surrounding Sojourn, to the west of Southern Cross and east and west of Matua that trend in the direction of absolute plate motion and are nearly continuous from west to east. The systematic residual provides compelling evidence that plate flexure due to seamount loading cannot account for the entire observed free-air anomaly.

[26] Sojourn lies within a residual FAA low (Figure 9c) that could be caused by a combination of crustal underplating and/or anomalously low density mantle. This broad low may be a continuation of one of the gravity lineaments that are well developed in the western part of the study area. The gravity lineaments decrease in amplitude to the east where the seafloor is younger. The decrease in amplitude, however, may be misleading. If these lineaments are caused by crustal underplating or mantle density variations that load the plate from below and if the rigidity of the plate increases with age, then the diminution toward the ridge could simply be an effect of a thinner plate rather than a change in subsurface density anomalies. For example, in older seafloor where the plate is stiffer, a low-density

anomaly in the mantle might not flex the plate significantly, so the combined effect of the gravitational attraction of the density anomaly and the muted topography created by flexure would be dominated by the density anomaly, creating a significant free-air gravity low. In young seafloor, the plate would flex more easily, creating elevated topography whose attraction would tend to cancel most of the attraction of the low-density anomaly itself. The characteristic flexural wavelength, where flexural stresses and the weight of the topography play equal roles in balancing the buoyant compensation, decreases from about 132 km when the effective elastic thickness is 8 km to about 47 km when T_e is 2 km. Thus the broader anomalies could be maintained by flexural rigidity in the older seafloor, but be isostatically compensated in younger seafloor.

5. Residual Mantle Bouguer Anomalies and Residual Topography

[27] To emphasize the subsurface density anomalies that may be responsible for the gravity lineaments and to show whether they continue into younger seafloor, we use residual mantle Bouguer anomalies (rMBA) instead of the free-air anomaly and also introduce the concept of residual topography. The residual mantle Bouguer anomaly is generated by subtracting from the mantle Bouguer anomaly the effects of thickening of the crust due to surface loading beneath the isolated volcanic edifices. The residual topography is generated by subtracting the effects of surface loading of the isolated volcanic edifices from the topography.

[28] The usual mantle Bouguer anomaly (MBA) subtracts from the FAA the attraction of the topography and an assumed crust of constant thickness and density overlying mantle of a constant density. The MBA is particularly useful in situations where some of the topography is formed by processes not involving changes in crustal structure, such as the dynamic topography in median valleys, the flexural bulge seaward of trenches, or the subsidence of seafloor with increasing age. In our case, there is both flexural topography surrounding seamounts and predictable crustal thickening beneath the seamount. To emphasize processes other than surface loading by seamounts, we calculate the rMBA by subtracting the attraction of the topography assuming constant crustal thickness and density everywhere except beneath the seamount edifices isolated by the median filter (Figure 4a); in those locations we assume the crustal thickness has been augmented by the height of the load.

[29] Again, we realize that the strength of the lithosphere should increase with age, but for simplicity, we have assumed a constant elastic thickness for the region. Later, we illustrate the effect that a greater T_e would have on crustal thickness and topography near the Southern Cross Seamount.

[30] To estimate the height of the load or additional thickness of crust beneath the seamount edifices due to flexure, we assume that the observed topography is the superposition of the surface volcanic load and the flexural response to the load, so that

$$L(k) = \frac{H(k)}{\left(1 - \Phi(k) \frac{(\rho_l - \rho_w)}{(\rho_m - \rho_w)}\right)} \quad (7)$$

where $L(k)$ is the Fourier transform of the load topography, $H(k)$ is the transform of the topography and $\Phi(k)$ is the flexural filter given in equation (3). Although this equation describes a linear relationship between H and L for a given rigidity, the problem is nonlinear because we wish to consider only positive (downward) loads restricted to the areas covered by seamount edifices. The usual harmonic expansion $L(k)$ has an indeterminate zero level (theoretically, there could be a uniform load everywhere as one component of the load) and allows both negative and positive topographic loads. If the zero level were set to zero, the average load over the whole region would be zero. We begin by assigning $L(k)$ to be the topography isolated by the median filter (Figure 4a), which is always ≥ 0 . For simplicity, we assumed a constant effective elastic thickness of 4 km, the average obtained from the inversions over individual features. We assume a density of the load of 2500 kg m^{-3} , because we believe that the best fitting density of 2300 kg m^{-3} assuming surface loading only is biased to the low side by subsurface loading. The thickness of material in the resulting flexural low beneath the seamounts was determined and added to the original seamount load. This larger load was then used to flex the 4 km plate and the thickness in the flexural low was reestimated. Because the loads are constrained to go to zero at the edges of the constructional edifices but the ridges are not entirely two-dimensional, introducing some asymmetry to the deflection, we subtract a linear trend connecting the edges from north to south at each step. The load was increased iteratively in this manner until the additional thickness added to the load was less than 1 m in height. The series converged rapidly, usually requiring less than 10 iterations to reach the 1 m height limit. This procedure gives us an estimate of flexure and crustal thickness beneath the edifices that we use in calculating rMBA and residual topography.

[31] The rMBA map shown in Figure 10 is dominated by continuous subparallel bands of negative anomalies roughly perpendicular to the EPR in the regions surrounding the major edifices. These lows are typically tens of kilometers across, with an amplitude of ~ 10 mGal. The lows are most pronounced along the Sojourn Ridge and in the vicinity of Matua Seamount. The lineament associated with the Sojourn Ridge appears to be continuous across the entire study region extending almost all the way to the EPR, while the lineament associated with the Hotu Matua volcanic complex and the northernmost part of the Rano Rahi seamount field appears to be discontinuous on 3–4 Ma seafloor, having nearly zero amplitude at -116°W , but it also continues nearly to the EPR. If we had adopted a density for the edifices was 2800 kg m^{-3} , as is often assumed for seamounts, instead of 2500, the rMBA low directly beneath the seamounts and Sojourn Ridge would have been more strongly negative. There are also a few residual highs of limited extent, the most obvious one at 11.6° S , 116.4° W , that are artifacts caused by seamounts that we did not survey and thus did not remove their predicted attraction from the free-air anomaly in generating the rMBA.

[32] In the calculation of the residual MBA we have neglected the shallow crustal contributions to the lateral variations in the density structure of the crust because they are expected to be small and there are no independent constraints on crustal variations in most of the study area.

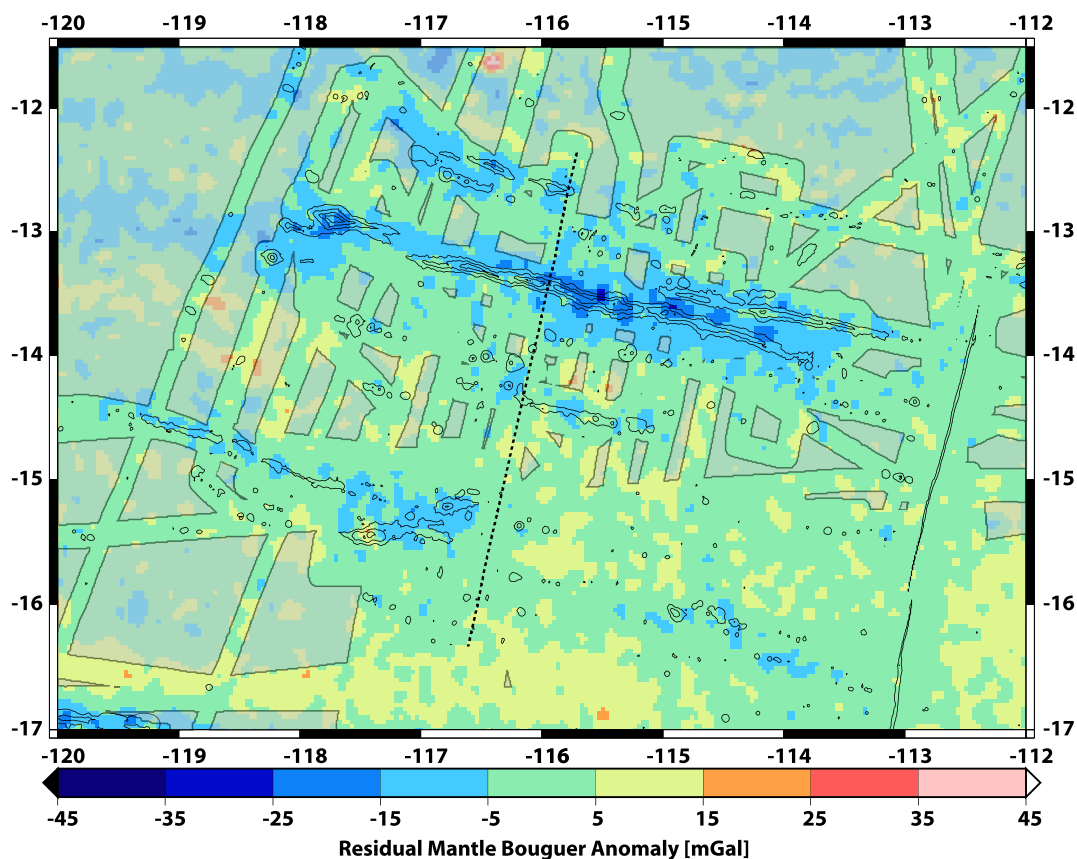


Figure 10. Residual mantle Bouguer anomaly generated by subtracting the attraction of the seamount edifices isolated by median filtering (Figure 4a), the predicted thickening of the crust beneath the isolated edifices, and the attraction of the remaining bathymetry (Figure 11) assuming constant crustal thickness for the residual bathymetry from the free-air anomaly. Black contours indicate the bathymetry contours at 800-m intervals, showing the major features in the region, while the dashed black line indicates the location of the GLIMPSE refraction line. There appears to be a banded pattern in the data, with gravity lows continuing from the west to the east to beneath the EPR. Unlike the map of the residual free-air anomalies (Figure 9c), this map reveals the attraction of the mass anomalies that isostatically compensate the longer-wavelength topographic features. In this model $\rho_w = 1030 \text{ kg m}^{-3}$, $\rho_l = 2500 \text{ kg m}^{-3}$, $\rho_{uc} = 2700 \text{ kg m}^{-3}$, $\rho_{lc} = 2900 \text{ kg m}^{-3}$, and $\rho_m = 3300 \text{ kg m}^{-3}$. The grayed transparent areas represent regions where no bathymetric data within 5 km exist.

For example, we have not accounted for sediments in flexural moats, rubble at the base of slopes, or variations in the crustal density. The shallow seismic reflection experiment during the Cook 16 leg of the R/V *Melville* revealed that sediment thickness in the flexural moats of the Sojourn ridge was approximately one hundred meters, with greater sediment thickness in the moat south of Sojourn than to the north; we estimate that the local gravity anomaly due to this thickness of sediment is approximately 2 mGal.

[33] The residual topography after calculating and removing the volcanic surface load and associated flexure from the observed topography provides more information on subsurface density anomalies. The surface load topography subtracted is the same used for the rMBA. With the nonlinear method we use for the calculation of the thickness of the surface load, when we subtract the thickness of the load and the resultant flexure, the anomalies directly beneath the edifices should linearly connect the values of residual topography on their south and north edges. However, because the scale of the remaining topography is small, many small,

narrow, along-track artifacts in the SeaBeam data become annoyingly visible. Consequently, we apply a low-pass filter with cutoff wavelength of 3 km to smooth the map, so the local maxima are not always right at the edges of the edifices (Figure 11).

[34] There is a ~ 200 km wavelength undulation of the residual seafloor topography (Figure 11), producing swells beneath the entire length of the Sojourn and Brown ridges, as well as the northernmost seamounts of the Rano Rahi group and the Hotu Matua volcanic complex. Surface loading and subsequent flexure cannot explain undulations with this wavelength. While a substantial portion of the map is within the median filter minimum of ± 50 m, there is a broad regional positive residual of more than 150 m in the areas over the Sojourn and Brown ridges as well as the Hotu Matua volcanic complex. The swells persist as far west as the SCSSM on seafloor that is at least 9 Ma, until our bathymetric coverage becomes too sparse to make definitive observations.

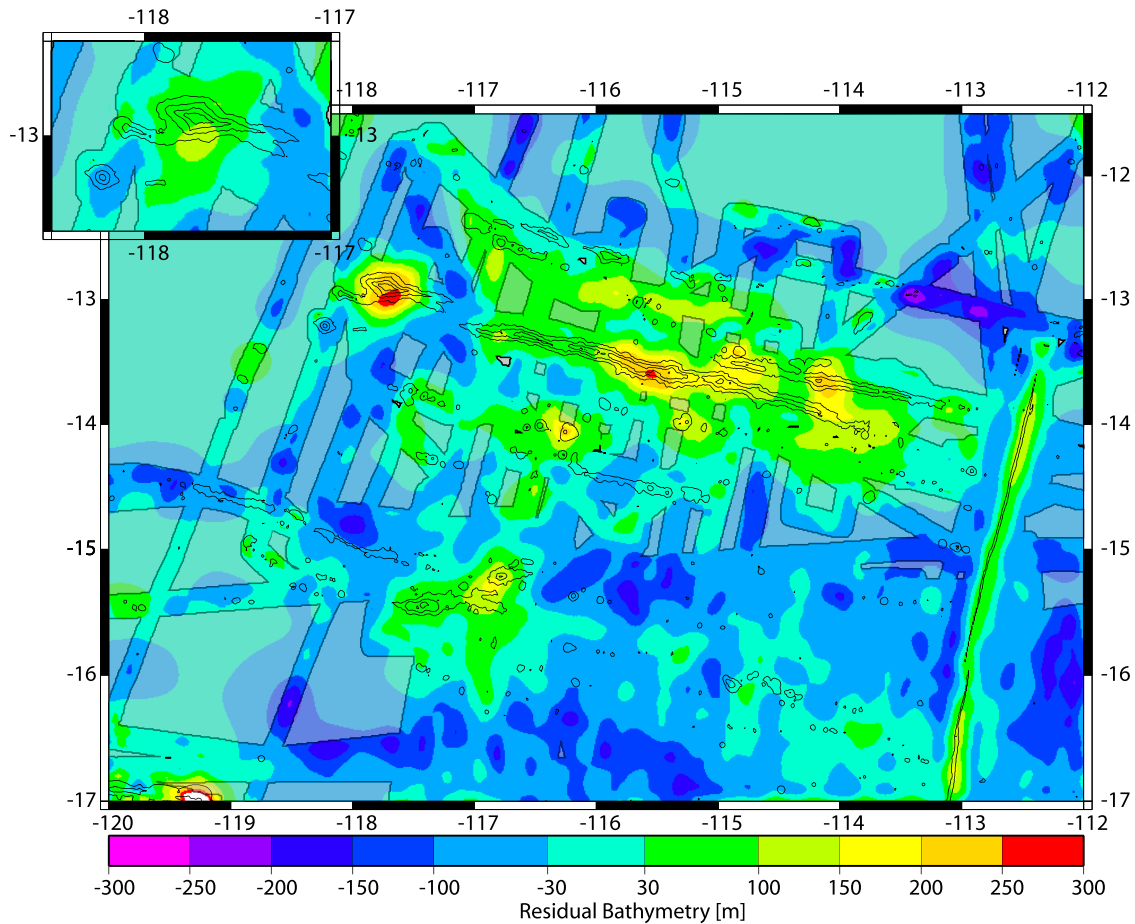


Figure 11. Residual bathymetry generated by subtracting from the bathymetry the isolated seamounts (Figure 4a) and associated flexure assuming surface loading on a plate with effective elastic thickness of 4 km. Low-pass filtering is applied to eliminate short-wavelength noise. The key features are the broad, residual highs in the region of the Sojourn and Hotu Matua ridge systems extending nearly to the EPR in the GLIMPSE study area. The inset map shows the residual topography around SCSM for an assumed elastic thickness of 8 km. The stronger plate reduces the amplitude and broadens the anomaly directly over the seamount. No reasonable combination of seamount density and elastic thickness can eliminate the broad, residual topographic swells. Black lines show original bathymetry at 800-m contour intervals. The grayed transparent areas represent regions where no bathymetric data within 5 km exists.

[35] How robust is the characterization of the topographic swells in the vicinity of the Sojourn Ridge and Hotu Matua Volcanic Complex? We consider two factors, reducing the assumed seamount load density and increasing the assumed plate rigidity, that would tend to reduce the magnitude of downward flexural deflections, which in turn would reduce the amplitude of our calculated residual topographic highs. For Sojourn Ridge, lowering the seamount density is incompatible with the short-wavelength free-air anomaly immediately above the edifice. Furthermore, as noted above, we are more likely to be underestimating the density of the ridge because of neglecting buoyant loads at the base of the plate (underplating), in which case removing the loading effect would leave a larger residual high. In the case of increasing the plate rigidity, to reduce residual topography swells at their wavelengths of ~ 200 km would require effective elastic thicknesses so large that the observed moats surrounding Sojourn Ridge and other large edifices could not be explained as flexural responses to their volcanic loads. An example is provided by the Southern Cross

Seamount. Here our earlier analyses indicate that the plate is stiffer than the assumed 4 km average value for the entire study area. The residual topography shows a ring of negative values surrounding a pronounced high (Figure 11). If we assign a greater elastic thickness, then the central high would be reduced in amplitude and the surrounding lows reduced or eliminated (inset, Figure 11). However, by searching a reasonable range of densities and elastic thicknesses that satisfy the FAA, no combination removes the broad positive residual bathymetry centered on Southern Cross.

[36] The positive residual bathymetry persists in regions with no significant surface loading, providing further evidence that the swells are not an artifact of insufficient modeling of flexural conditions. For example, the region immediately south of the easternmost Brown Ridge and the region west of the EPR at 16–17°S are two such areas where there are positive residuals without large seamounts and substantial flexure. In these regions we are subtracting an essentially flat plane from the age-detrended seafloor.

Therefore we conclude that the swells are robust features that are modulated by the effective elastic thickness and the seamount density and are not an artifact of those parameters.

[37] Simple explanations for the broad residual topography undulations and residual MBA anomalies include buoyant material in the shallow mantle or crustal underplating. The GLIMPSE seismic refraction/wide-angle reflection experiment (Holmes et al., submitted manuscript, 2006) provides an independent constraint on the extent of crustal underplating along line d in Figure 3 crossing the Sojourn Ridge and extending south past the Hotu Matua trend to 16°S. In particular, the seismic profile shows ~700 m thicker crust in a broad band about 100 km across approximately centered on the Sojourn Ridge. There is a small amount of local downwarping beneath the ridge, but nothing resembling local isostatic compensation of that narrow feature. As we show below, this amount of crustal thickening can only account for about half of the broad anomalies in elevation and gravity flanking the Sojourn. Rayleigh wave tomography and body wave delays demonstrate that there are also bands of anomalously low P and S wave velocities in the mantle beneath Sojourn and Hotu Matua [Weeraratne et al., 2003a, D. Weeraratne et al., Rayleigh wave tomography of the oceanic mantle beneath intraplate seamount chains in the South Pacific, submitted to *Journal of Geophysical Research*, 2006, hereinafter referred to as Weeraratne et al., submitted manuscript, 2006; Harmon et al., submitted manuscript, 2006] presumably corresponding to hotter, low-density material that provides the rest of the compensation.

[38] Gravity and topography data alone cannot uniquely constrain the depth of compensation accurately enough to distinguish between crustal underplating and shallow mantle anomalies, but we can test whether a flexural model of isostasy is consistent with both the undulation of the seafloor and the gravity of the Sojourn Ridge. We model a stacked profile of bathymetry and shipboard gravity (Figure 12), compiled from six individual profiles across the ridge (Figure 3). A series of 2-D inversions of this profile provides some constraints on the flexural rigidity and lateral distribution of anomalous densities. We allow both surface and subsurface loads and explore a family of models with laterally varying rigidity to see whether there is any indication that the plate is broken beneath the ridge or is thinned in the vicinity of the ridge. Near the Thanksgiving seamounts, there may be errors in the gravity stacks due to lack of two-dimensionality, because the two profiles across this small seamount chain cross it near the end and at its highest point. The gravity signal there is asymmetric and smaller than expected for the size of the stacked topography. Otherwise, the stacked gravity data and stacked topography data appear self-consistent. To model the fourth-order differential equation describing flexure of a variable-thickness elastic plate overlying an inviscid fluid we used a fifth-order accurate finite difference approximation, and we inverted for surface and subsurface loading using a weighted least squares scheme. To explore the broken plate model, we allowed the elastic thickness in the region to thin smoothly from the edges of model to nearly zero elastic thickness beneath the Sojourn ridge over a given distance that we varied in different trials. The results of this model agree with theory that predicts a ~33% narrower flexural moat for the broken

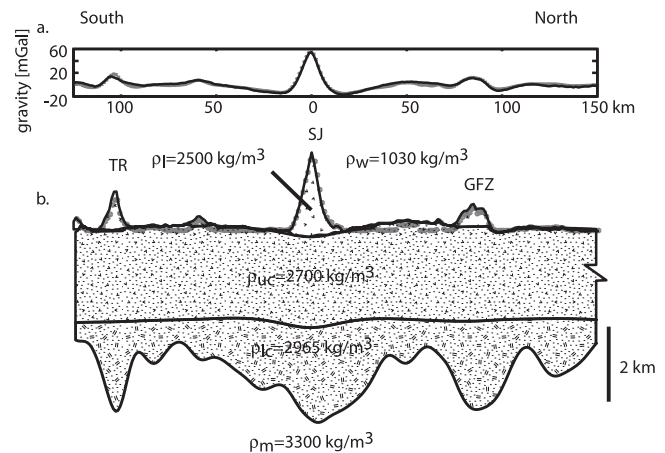


Figure 12. Inversion of a stacked topography and gravity profile across the Sojourn Ridge for surface and subsurface (Moho) loads. Stacked profile includes lines c–f in Figure 3. (a) Observed (solid black line) and predicted (dotted grey line) free-air gravity anomaly of our best fitting model. (b) Observed (uppermost solid black line) and predicted (dotted grey line) surface topography. Solid line immediately beneath the ridges and seamounts shows the base of the model surface load; surface loading is allowed only where seamounts were isolated by the median filter (Figure 4a). Subsurface loading (deepest shaded region) in the form of crustal underplating beneath an initially uniform thickness crust is allowed everywhere. Effective elastic thickness is assumed to be 4 km. TR, Thanksgiving Ridge; SJ, Sojourn Ridge; and GFZ, Garrett Fracture Zone. The form of the subsurface load in the vicinity of the Garrett fracture zone is probably spurious because we expect a contrast in mantle density across the fracture zone due to change in age of the lithosphere. There is general overall agreement with the GLIMPSE refraction study of Holmes et al. (submitted manuscript, 2006) over the TR and SJ, i.e., thickening of the crust over a region broader than the edifice. The density structure shown is based on a modified version of Carlson and Herrick's [1990] relationship for translating seismic velocities to density in basaltic crust to be comparable to Holmes et al. (submitted manuscript, 2006).

plate [Turcotte and Schubert, 2002] than that predicted by a uniform thickness plate, provided the thickness remains constant. Assuming only surface loading, the fit to the data is slightly worse for the best broken plate model (6 km–0.1 km over 40 km half width, RMS errors of 125 m and 3.2 mGal) than for a uniform thickness (4 km, RMS errors of 96 m and 3.5 mGal), and the narrower moats are unable to match both the observed topography and free-air gravity anomaly. In contrast to the models discussed in earlier sections and illustrated in Figures 5–8 that may have both positive and negative surface loads distributed anywhere in order to exactly match the topography, surface loads in this section are required to be positive and confined to the edifices themselves. These restricted, nonlinear models consequently have misfits to both gravity and topography data. Modifying the distance over which the fall off occurred or the maximum thickness does not produce a model that fits better than a uniform plate. Our goal in these model experiments was to look for the surface loading model that yields the maximum

variance reduction of the observations, thus yielding the minimum estimate of the required subsurface contribution to the topography and gravity anomalies. Consequently, we reaffirm our choice of the standard flexural model over the broken plate model for the calculation of the residual MBA. The model presented in Figure 12 illustrates the introduction of a subcrustal load to produce a residual swell beneath the Sojourn Ridge. We use a 4 km uniform elastic thickness for the purpose of this illustration but models where the plate stiffens away from the Sojourn ridge are also acceptable. Specifically, for a 40 km half width falloff in elastic thickness beneath Sojourn ridge, we found that the eroded lithosphere model (thinning from 8 km to 2 km) produced RMS errors of 69 m and 1.9 mGal; the broken plate model (thinning from 6 km to 0.1 km) yielded RMS errors of 83 m and 2.1 mGal. The 4 km uniform elastic thickness model yielded RMS errors of 71 m and 2.2 mGal. With the addition of subsurface loading, we thus substantially reduce the misfit in the topography and the gravity data compared to surface loading alone (Figure 12). The surface loads again are required to be positive and limited to the seamounts isolated from the observed bathymetry. The form of the inferred subsurface load in this case is thickened crust beneath the major edifices, with asymmetric loading to the north of Sojourn. The results of this inversion are similar to the refraction data, and satisfy the topography and the gravity constraints better than surface loading alone. Notably, the residual topography over Sojourn Ridge has been reduced to less than 100 m; consistent with the depth of sediment in the region, and the gravity residual is a low-amplitude negative beneath Sojourn with wavelengths on the order of 150–200 km. This remaining small residual anomaly (~5 mGal) could be indicative of low-density anomalies in the asthenosphere that do not fully transmit their buoyancy to the overlying plate. Attributing all of the subsurface loading to crustal underplating represents one end-member of the range of possible models. This inversion shows that approximately 1.5 km of average thickening is required in a region 100 km across, roughly double that found along the seismic refraction profile, in agreement with the Rayleigh wave observations (Weeraratne et al., submitted manuscript, 2006) indicating a mantle anomaly that is probably responsible for part of the subsurface load.

[39] There is one caveat to the addition of subsurface loading into the model. The subsurface load will directly affect the estimation of effective elastic thickness in the region. The most direct and artificial effect, in the case of the buoyant subsurface load presented here will be to reduce the total free-air anomaly over the seamounts and ridges, giving the perception of more compensation at depth and lower estimates for effective elastic thickness, as was the case for Matua. Another physical effect occurs if the load results from a thermal anomaly, where thermal erosion of the lithosphere would reduce the effective elastic thickness. These two effects indicate that our estimates are minimum values of elastic thickness for the age of the seafloor loaded by the seamounts. The presence of subsurface loading beneath Pacific seamounts might explain the consistently low estimates for elastic thickness throughout the region, as has previously been suggested for the Cross Grain and Puka

ridges [McAdoo and Sandwell, 1989; Goodwillie, 1995].

6. Implications for the Origin of Volcanic Ridges

[40] Three types of mechanisms have been invoked for lithospheric production of the gravity lineaments and the associated volcanism: diffuse extension producing lithospheric boudinage or stretching [Winterer and Sandwell, 1987], lithospheric cracking through hydrofracture [Hieronymus and Bercovici, 2000], and cracking due to thermal contraction [Sandwell and Fialko, 2004; Gans et al., 2003]. The boudinage model has fallen out of favor because fixed fracture zone separation across the Pacific plate indicates there has been insufficient strain normal to the absolute plate motion to produce the lithospheric thinning required by the diffuse extension model [Goodwillie and Parsons, 1992; Gans et al., 2003]. The boudinage model also predicts volcanism where the crust has been thinned by extension, in opposition to the observation in this paper that crustal thickening is required beneath the ridges to satisfy gravity and topography observations. In addition, we have shown the intraplate volcanism lies atop a broad swell, whereas the boudinage model predicts the seamount chains to be built on topographic lows. These observations allow us to reject the boudinage model.

[41] Fundamentally, both of the cracking models are governed by lithospheric flexure: the gravity anomaly is produced by topography from flexure of the plate without any significant alteration of lithospheric structure. The tapping of a ubiquitous reservoir of asthenospheric melt produces the volcanic seamount chains. The differences in the models are in the driving force that produces the cracking. Hieronymus and Bercovici [2000] used a combination of membrane stresses, flexural stresses associated with self-loading of seamounts, and regional tectonic stresses, along with an ample supply of melt, to produce a crack in the lithosphere propagated by hydrofracture. The thermal cracking models use the lateral contraction and flexural warping of the cooling lithosphere to produce the observed wavelengths and amplitudes in the satellite free-air anomaly [Gans et al., 2003; Sandwell and Fialko, 2004].

[42] Both models can explain the orientation of the volcanic ridges, provided there are remotely applied, regional extensional stresses oriented perpendicular to the APM direction. However, the self-loading model cannot explain the orientation or existence of gravity lineaments in the absence of volcanism. If linear, volcanic loads such as Sojourn Ridge are generated through some other mechanism, however, the stresses induced could organize flexure and cracking in a much broader region [Karner and Weissel, 1990].

[43] Lithospheric cracking models require the extraction of volumes of preexisting melt from the asthenosphere. In addition to the volume of the edifices themselves, our modeling of the residual mantle Bouguer anomaly indicates that there may be two kilometers or more of crustal thickening beneath the Sojourn Ridge and/or anomalously low densities in the mantle distributed across a region tens of km wide. The seismic refraction/reflection data (Holmes et al., submitted manuscript, 2006) indicate that at least some of source of the rMBA is crustal thickening. Without

some dynamic mechanism for concentrating melt, it is implausible that a sufficient volume can be gathered to create several kilometers of crust from the 1–2% or less melt fraction that may be distributed within the asthenosphere. In addition, the siphoning of partial melt from the underlying asthenosphere should produce a denser residuum beneath the volcanic lineaments, because the liquid phase that is removed is less dense than the matrix. This removal of preexisting melt is different than upwelling beneath a mid-ocean ridge, where the process of creating additional melt leaves a depleted residuum that is less dense than the mantle before initial melting. If the mantle were more dense beneath the volcanic ridges, then it would require even greater crustal thickening through underplating to mask its gravity signature, further exacerbating the problem of extracting a large enough volume of melt by requiring additional melt to be present.

[44] The thermoelastic flexure and cracking hypothesis predicts that the seafloor should be dynamically depressed before or synchronously with volcanism, with no crustal thickening or alteration of the mantle lithosphere and therefore no residual mantle Bouguer anomaly. A positive rMBA would be expected if enough low-density melt were withdrawn from the asthenosphere. We find the opposite. After subtracting the effects of the surface loading represented in the volcanic edifices, there is a residual topographic swell and a pronounced, negative, residual mantle Bouguer anomaly along the volcanic lineaments. The dispersion of Rayleigh waves [Weeraratne et al., 2003a, also submitted manuscript, 2006] indicates that at least some of the source of the rMBA is within the shallow mantle. If sufficient melt could be extracted in the cracking model to supply underplated crust, uplift in the vicinity of a crack in the downward flexed lithosphere is possible, contrary to the simple cartoon predictions. However, the cracking model for the origin of volcanic ridges is not consistent with the major seismological anomalies we have observed in other components of the GLIMPSE study. Although we do not favor the lithospheric cracking models as the primary origin of the volcanic ridges and gravity lineaments, cracking and self-loading by seamounts can clearly influence the transport of magma to the surface, perhaps explaining the en echelon nature of some of the ridge systems [Winterer and Sandwell, 1987; Sandwell et al., 1995; Lynch, 1999; Forsyth et al., 2006] if a remotely applied stress field is not exactly perpendicular to the overall trend of the volcanic activity.

[45] We think the patterns of topographic swells, rMBAs and crustal thickness are best explained by models inspired by the small-scale convection models of Buck and Parmentier [1986] and Haxby and Weissel [1986]. In their models, the cooling lower part of the lithosphere becomes gravitationally unstable and initiates convection that is subsequently organized into convective rolls oriented in the APM direction by the shear between the plate and the underlying deeper mantle [Richter and Parsons, 1975]. The upwelling limbs of the convection cells can provide the needed volume of melt by decompression melting. Underplated crust, the low density of the upwelling mantle and a more depleted, less dense residual mantle could all contribute to the buoyancy generating the topographic swell and negative residual Bouguer anomalies. In older lithosphere in the western part of our study area, the

increased flexural rigidity could suppress the topographic swells, so that low-density mantle would be expressed primarily in both rMBA and FAA lows that connect to the residual topographic swells in younger seafloor. The thicker lithosphere might also be more resistant to penetration by magma. Convective models can match the observed wavelengths of the gravity lineaments [Buck and Parmentier, 1986], and are viable candidates for the explanation of both the lineaments and the associated intraplate volcanism. Nevertheless, there is one feature of these models that apparently contradicts one of the observations made here.

[46] One of the key requirements for small-scale convection initiated by cooling from above is time for the instabilities to form. Estimates of the time required range from several to tens of millions of years [Davaille and Jaupart, 1994; Korenaga and Jordan, 2003], depending on the viscosity of the asthenosphere and the thickness of the density-stratified uppermost mantle created at the spreading center. If the temperature-dependent viscosity reaches a minimum of about 10^{17} Pa s, convection could initiate within a few hundred kilometers of the East Pacific Rise [Buck and Parmentier, 1986; Barnouin-Jha and Parmentier, 1997; Marquart et al., 1999; Marquart, 2001; Zaranek and Parmentier, 2004]. We observe gravity anomalies in the rMBA extending continuously in the case of the Sojourn Ridge eastward all the way to the EPR or zero age seafloor; this observation is inconsistent with the onset time requirement. In addition, the nearly continuous rMBA anomalies over the Hotu Matua complex also extend back to the EPR, and the Puka Puka ridge extends nearly to the East Pacific Rise along the central Rano Rahi seamounts.

[47] With the loss of some parsimony, the small-scale convection model can be fit to these observations. We propose that the Garrett fracture zone to the north of the Sojourn Ridge could induce convection by juxtaposing cooler material north of the fracture zone with warmer material south of the fracture zone. Numerical models indicate that fracture zones can organize small-scale convection and induce it much sooner than beneath lithosphere with no age offsets [Robinson et al., 1988; Marquart et al., 1999; Huang et al., 2003]. The facts that the Sojourn ridge is the largest and most continuous of the intraplate ridges in this part of the Pacific and the Southern Cross/Sojourn/Brown system extends no further west than the point where the Garrett fracture zone began [Goff and Cochran, 1996; Forsyth et al., 2006] may indicate that such fracture zone-induced convection plays an important role. The continuation of the Hotu Matua and Puka Puka trends to the EPR, however, requires an additional explanation. None of the models of small-scale convection have considered the role of return flow in the asthenosphere back toward the ridge. Several lines of evidence have led to the suggestion that return flow west of the East Pacific Rise in this area is unusually strong, perhaps representing flow from the Pacific Superswell region [Phipps Morgan et al., 1995; Phipps Morgan, 1997; Forsyth et al., 1998; Toomey et al., 2002; Conder et al., 2002; Gaboret et al., 2003]. It is possible that small-scale convection initiates off-axis and then is carried back toward the ridge in the return flow field.

[48] One indication that return flow may play an important role is the existence of isotopic anomalies along the

East Pacific Rise where the Hotu Matua and Rano Rahi trends intersect the spreading center [Mahoney *et al.*, 1994; Kurz *et al.*, 2005]. These isotopic anomalies lie along the same mixing trend found in Puka Puka and Hotu Matua [Janney *et al.*, 2000; Donnelly *et al.*, 2003], with degree of enrichment tending to decrease toward the EPR. It may be that anomalously enriched mantle is introduced into the asthenosphere by upwelling at hot spots and then is swept back toward the spreading center in the return flow. The compositional heterogeneities may play an active role in controlling the pattern of flow and in generating or initiating the melting leading to formation of the intraplate volcanic ridges. A pressure gradient is required to drive return flow, which can be created by the buoyancy of the hot spots in the superswell region. If the upwelling mantle is less viscous than the ambient asthenosphere due to higher temperatures and/or higher water content, then Saffman-Taylor (viscous fingering) instabilities may form because flow in an asthenospheric layer requires less work if it is concentrated in low-viscosity channels. Shear between the overlying plate and the subasthenosphere mantle may organize the fingers into channels oriented in the direction of absolute plate motion [Weeraratne *et al.*, 2003b]. Thus the fingers can be source of compositional heterogeneities oriented perpendicular to the EPR and/or conduits for increased return flow. As the plate thins toward the EPR, the asthenospheric channel may shallow, introducing a small component of upwelling that could cause small amounts of pressure release melting or occasionally trigger convective overturn and more extensive, local melt production [Raddick *et al.*, 2002]. Even if no melting is induced, higher temperatures or compositional differences could create density differences that would be carried back to the spreading center. The existence of heterogeneities in the return flow could thus be responsible for the continuation of gravity and topographic anomalies from older seafloor into very young seafloor adjacent to the East Pacific Rise.

[49] This discussion of the volcanic ridges centers around the hypothesis that they originate from the same process as the gravity lineaments. Although the Puka Puka, Hotu Matua and Sojourn trends all lie in gravity lows, not all gravity lows have associated volcanic ridges. It is possible that the volcanic ridges originate from some other process and their presence just helps organize lithospheric stresses that create the nonvolcanic lineaments. Thus, although we are confident in concluding that the ridges are not created by the passive tapping of asthenospheric melt by lithospheric cracking, the generalization that the overall pattern of gravity lineaments is caused by an asthenospheric process is less certain. A similar study of bathymetry, gravity, and seismic structure is needed in an area in which there is no significant volcanism accompanying the gravity lineaments.

7. Conclusions

[50] 1. Assuming only surface loading of an elastic plate, we estimate an average density of seamounts and volcanic ridges of about 2400 kg m^{-3} , slightly lower than expected. While high porosity in the basaltic crust could contribute to the apparent low density, extremely low density estimates for Matua and Southern Cross seamounts and a seismic refraction/wide-angle reflection profile across the Sojourn

ridge suggest that the chief cause of the anomalous estimates is subsurface loading of the plate, primarily in the form of crustal underplating.

[51] 2. The apparent elastic thickness of the lithosphere assuming surface loading ranges from 2 to 10 km, within the range expected for seafloor of 3–9 Ma, although most estimates are nearer the lower bound. There appears to be no significant increase in elastic thickness with age with the exception of Southern Cross seamount; we assume that some edifices, such as Hotu seamount, formed near the EPR on weak lithosphere and had the flexural signature “frozen in”. Other edifices show evidence for recent volcanism, such as Matua seamount which is forming on ~6 Ma seafloor, or have Ar/Ar ages that indicate they could not have formed on very young seafloor. Low estimates for elastic thickness in these regions could be due to thermal erosion of the elastic lithosphere, but there may also be a systematic bias toward anomalously low rigidities introduced by the neglect of subsurface loading.

[52] 3. Locally, counting both the edifice and the apparent crustal underplating, the crust may be doubled in thickness from an average of ~6 km. The total volume of crustal underplating may be greater than the volume of the surface loading represented in the seamounts.

[53] 4. After subtracting from the free-air anomaly the optimal estimate of the effects of topography and its flexural compensation, assuming surface loading only, the residual free-air gravity anomaly exhibits systematic negative anomalies in the vicinity of the Sojourn and Hotu Matua ridge systems. Although much of the free-air anomaly low flanking the Sojourn ridge is attributable to flexure, these residual anomalies indicate that a model of surface loading and plate flexure cannot alone account for the observed gravity lineaments in the GLIMPSE study region.

[54] 5. The rMBA has systematic lows associated with the Sojourn and Hotu Matua ridge systems. These lows are nearly continuous from the western edge of the study area to the EPR, trend roughly in the spreading direction, and are tens of kilometers wide. The rMBA indicates there is subsurface loading from anomalously low densities beneath these two ridge systems. Seismic refraction/wide-angle reflection and surface wave tomography indicates that this buoyant material is probably a combination of crustal underplating and low densities in the shallow mantle.

[55] 6. The residual bathymetry shows that there are broad topographic highs associated with the Sojourn and Hotu Matua ridge systems. Superimposed on the broad highs are the edifices themselves and the flexural response to the edifices, smaller in scale but analogous to the Hawaiian swell with the Hawaiian islands and their flexural moats.

[56] 7. Finally, we have used the aforementioned observations and interpretations to test the various hypotheses proposed for the formation of the gravity lineaments and the associated intraplate volcanic ridges. We find that the combination of swell topography and negative rMBA anomalies beneath the ridge systems contradict lithospheric cracking models which predict no mantle density anomalies and negative topography beneath the ridges. Our observations are most consistent with mantle dynamic models involving upwelling, such as small-scale convection which could be initiated on young seafloor by juxtaposition with

older lithosphere at fracture zones and organized by the shearing between the plate and the deeper mantle. This suite of models predict that the ridges should be underlain by low-density mantle, sit on topographic swells, trend in the absolute plate motion direction, and locally produce a large volume of magma through decompression melting. The existence of low-density material in the mantle beneath the ridges is corroborated by low seismic velocities observed by Rayleigh wave dispersion and inferred from body wave delays whose magnitudes are too large to be explained by crustal thickening alone. The extension of the residual swells and mantle Bouguer anomalies almost all the way back to the East Pacific Rise, the asymmetry of seamount populations and gravity lineaments across the spreading center, the asymmetric subsidence of the seafloor, and the existence of geochemical anomalies along the EPR that follow the same mixing trend all suggest that return flow in the asthenosphere from the Pacific Superswell region back to the EPR plays an important role, either in transporting compositional heterogeneities that trigger melting or in carrying small-scale convective swells closer to the mid-ocean ridge, or both.

[57] **Acknowledgments.** We would like to thank the captain and crew of the R/V *Melville* for legs Cook 16 and Vancouver 4 for their outstanding performance during the first and second legs of the experiment, Chad Holmes for providing us with the refraction data, and David Sandwell, Douglas Wilson, and Roger Buck for their thoughtful reviews and their active participation in the ongoing debate over the origin of the lineaments. This work was funded by NSF OCE-9911729.

References

- Barnouin-Jha, K., and E. M. Parmentier (1997), Buoyant mantle upwelling and crustal production at oceanic spreading centers: On-axis and off-axis melting, *J. Geophys. Res.*, *102*, 11,979–11,989.
- Baudry, N., and L. W. Kroenke (1991), Intermediate-wavelength (400–600 km), South Pacific geoidal undulations: Their relationship to linear volcanic chains, *Earth Planet. Sci. Lett.*, *102*, 430–443.
- Buck, W. R., and E. M. Parmentier (1986), Convection beneath young oceanic lithosphere; implications for thermal structure and gravity, *J. Geophys. Res.*, *91*, 1961–1974.
- Calmant, S., and A. Cazenave (1986), The effective elastic lithosphere under the Cook-Austral and Society islands, *Earth Planet. Sci. Lett.*, *77*, 187–202.
- Calmant, S., and A. Cazenave (1987), Anomalous elastic thickness of the oceanic lithosphere in the south-central Pacific, *Nature*, *328*, 236–238.
- Carlson, R. L., and C. N. Herrick (1990), Densities and porosities in the oceanic crust and their variations with depth and age, *J. Geophys. Res.*, *95*, 9153–9170.
- Cazenave, A., S. Houry, B. Lago, and K. Dominh (1992), Geosat-derived geoid anomalies at medium wavelength, *J. Geophys. Res.*, *97*, 7081–7096.
- Cazenave, A., B. Parsons, and P. Calcagno (1995), Geoid lineations of 1000 km wavelength over the central Pacific, *Geophys. Res. Lett.*, *22*, 97–100.
- Cochran, J. R. (1986), Variations in subsidence rates along intermediate and fast spreading mid-ocean ridges, *Geophys. J. R. Astron. Soc.*, *87*, 421–459.
- Conder, J. A., D. W. Forsyth, and E. M. Parmentier (2002), Asthenospheric flow and asymmetry of the East Pacific Rise, MELT area, *J. Geophys. Res.*, *107*(B12), 2344, doi:10.1029/2001JB000807.
- Davaille, A., and C. Jaupart (1994), Onset of convection in fluids with temperature-dependent viscosity: Application to the oceanic mantle, *J. Geophys. Res.*, *99*, 19,853–19,866.
- Donnelly, K. E., C. H. Langmuir, and S. L. Goldstein (2003), Geochemical constraints on melting process in the GLIMPSE region, *Eos Trans. AGU*, *84*(46), Fall Meet. Suppl., Abstract V21B-05.
- Drafer, N. R., and H. Smith (1998), *Applied Regression Analysis*, 708 pp., John Wiley, Hoboken, N. J.
- Filmer, P. E., M. K. McNutt, and C. J. Wolfe (1993), Elastic thickness of the lithosphere in the Marquesas and Society Islands, *J. Geophys. Res.*, *98*, 19,565–19,577.
- Fleitout, L., and C. Moriceau (1992), Short-wavelength geoid, bathymetry and the convective pattern beneath the Pacific Ocean, *Geophys. J. Int.*, *110*, 6–28.
- Forsyth, D. W. (1985), Subsurface loading and estimates of the flexural rigidity of continental lithosphere, *J. Geophys. Res.*, *90*, 12,623–12,632.
- Forsyth, D. W., et al. (1998), Imaging the deep seismic structure beneath a mid-ocean ridge; the MELT experiment, *Science*, *280*, 1215–1218.
- Forsyth, D. W., N. Harmon, and D. S. Scheirer (2006), Distribution of recent volcanism and the morphology of seamounts and ridges in the GLIMPSE study area: Implications for the lithospheric cracking hypothesis for the origin of intraplate, non-hot spot volcanic chains, *J. Geophys. Res.*, *111*, B11407, doi:10.1029/2005JB004075.
- Gaboret, C., A. M. Forte, and J. P. Montagner (2003), The unique dynamics of the Pacific hemisphere mantle and its signature on seismic anisotropy, *Earth Planet. Sci. Lett.*, *208*, 219–233.
- Gans, K. D., D. S. Wilson, and K. C. Macdonald (2003), Pacific plate gravity lineaments: Diffuse extension or thermal contraction?, *Geochem. Geophys. Geosyst.*, *4*(9), 1074, doi:10.1029/2002GC000465.
- Goff, J. A., and J. R. Cochran (1996), The Bauer Scarp ridge jump: A complex tectonic sequence revealed in satellite altimetry, *Earth Planet. Sci. Lett.*, *141*(1–4), 21–33.
- Goodwillie, A. M. (1995), Short-wavelength gravity lineations and unusual flexure results at the Puka Puka volcanic ridge system, *Earth Planet. Sci. Lett.*, *136*, 297–314.
- Goodwillie, A. M., and B. Parsons (1992), Placing bounds on lithospheric deformation in the central Pacific Ocean, *Earth Planet. Sci. Lett.*, *111*, 123–139.
- Grevenmeyer, I., and E. R. Flueh (2000), Crustal underplating and its implications for subsidence and state of isostasy along the Ninetyeast Ridge hotspot trail, *Geophys. J. Int.*, *142*, 643–650.
- Grevenmeyer, I., W. Weigel, S. Schuessler, and F. Avedik (2001), Crustal and upper mantle seismic structure and lithospheric flexure along the Society Island hotspot chain, *Geophys. J. Int.*, *147*, 123–140.
- Grevenmeyer, I., B. Schramm, C. W. Devey, D. S. Wilson, B. Jochum, J. Hauschild, K. Aric, H. W. Villinger, and W. Weigel (2002), A multibeam-sonar, magnetic and geochemical flowline survey at 14°14'S on the southern East Pacific Rise: Insights into the fourth dimension of ridge crest segmentation, *Earth Planet. Sci. Lett.*, *199*, 359–372.
- Hammer, P. T. C., J. A. Hildebrand, and R. L. Parker (1991), Gravity inversion using seminorm minimization; density modeling of Jasper Seamount, *Geophysics*, *56*, 68–79.
- Hammer, P. T. C., L. M. Dorman, J. A. Hildebrand, and B. D. Cornuelle (1994), Jasper Seamount structure; seafloor seismic refraction tomography, *J. Geophys. Res.*, *99*, 6731–6752.
- Harrison, J. C., and W. C. Brisbin (1959), Seamount Jasper: 1. Gravity anomalies off the west coast of North America, *Geol. Soc. Am. Bull.*, *70*, 929–933.
- Haxby, W. F., and J. K. Weissel (1986), Evidence for small-scale mantle convection from Seasat altimeter data, *J. Geophys. Res.*, *91*, 3507–3520.
- Hieronimus, C. F., and D. Bercovici (2000), Non-hotspot formation of volcanic chains: Control of tectonic and flexural stresses on magma transport, *Earth Planet. Sci. Lett.*, *181*, 539–554.
- Huang, J., S. Zhong, and J. van Hunen (2003), Controls on sublithospheric small-scale convection, *J. Geophys. Res.*, *108*(B8), 2405, doi:10.1029/2003JB002456.
- Hyndman, R. D., N. I. Christensen, and M. J. Drury (1979), Seismic velocities, densities, electrical resistivities, porosities and thermal conductivities of core samples from boreholes into the islands of Bermuda and the Azores, in *Deep Drilling Results in the Atlantic Ocean: Ocean Crust, Maurice Ewing Ser.*, vol. 2, edited by M. Talwani, C. G. Harrison, and D. E. Hayes, pp. 94–112, AGU, Washington, D. C.
- Ishihara, T. (1987), Gravimetric determination of densities of seamounts along the Bonin Arc, in *Seamounts, Islands, and Atolls*, *Geophys. Monogr. Ser.*, vol. 43, edited by B. H. Keating et al., pp. 97–113, AGU, Washington, D. C.
- Janney, P. E., J. D. Macdougall, J. H. Natland, and M. A. Lynch (2000), Geochemical evidence from the Pukapuka volcanic ridge system for a shallow enriched mantle domain beneath the South Pacific Superswell, *Earth Planet. Sci. Lett.*, *181*(1–2), 47–60.
- Karner, G. D., and J. K. Weissel (1990), Factors controlling the location of compressional deformation of oceanic lithosphere in the central Indian Ocean, *J. Geophys. Res.*, *95*, 19,795–19,810.
- Korenaga, J., and T. H. Jordan (2003), Linear stability analysis of Richter rolls, *Geophys. Res. Lett.*, *30*(22), 2157, doi:10.1029/2003GL018337.
- Korenaga, J., and T. H. Jordan (2004), Physics of multiscale convection in Earth's mantle: Evolution of sublithospheric convection, *J. Geophys. Res.*, *109*, B01405, doi:10.1029/2003JB002464.
- Kurz, M. D., M. Moreira, J. Curtice, L. E. Dempsey, J. J. Mahoney, and J. M. Sinton (2005), Correlated helium, neon, and melt production on the super-fast spreading East Pacific Rise, *Earth Planet. Sci. Lett.*, *232*, 125–142.
- Lynch, M. A. (1999), Linear ridge groups; evidence for tensional cracking in the Pacific plate, *J. Geophys. Res.*, *104*, 29,321–29,333.

- Lyons, S. N., D. T. Sandwell, and W. H. F. Smith (2000), Three-dimensional estimation of elastic thickness under the Louisville Ridge, *J. Geophys. Res.*, *105*, 13,239–13,252.
- Mahoney, J. J., J. M. Sinton, M. D. Kurz, J. D. Macdougall, K. J. Spencer, and G. W. Lugmair (1994), Isotope and trace element characteristics of a super-fast spreading ridge; East Pacific Rise, 13–23°S, *Earth Planet. Sci. Lett.*, *121*, 173–193.
- Maia, M. (2006), Comparing the use of marine and satellite data for geodynamic studies, paper presented at 15 Years of Progress in Radar Altimetry Symposium, Eur. Space Agency, Venice.
- Maia, M., and M. Diament (1991), An analysis of the altimetric geoid in various wavebands in the central Pacific Ocean: Constraints on the origin of intraplate features, in *The Geology, Geophysics and Metallogeny of the Present-Day Oceans*, pp. 133–153, Elsevier, New York.
- Marquart, G. (2001), On the geometry of mantle flow beneath drifting lithospheric plates, *Geophys. J. Int.*, *144*, 356–372.
- Marquart, G., H. Schmeling, and A. Braun (1999), Small-scale instabilities below the cooling oceanic lithosphere, *Geophys. J. Int.*, *138*, 655–666.
- McAdoo, D. C., and D. T. Sandwell (1989), On the source of cross-grain lineations in the central Pacific gravity field, *J. Geophys. Res.*, *94*, 9341–9352.
- McNutt, M. K., and A. V. Judge (1990), The superswell and mantle dynamics beneath the South Pacific, *Science*, *248*, 969–975.
- Minshull, T. A., and P. Charvis (2001), Ocean island densities and models of lithospheric flexure, *Geophys. J. Int.*, *145*, 731–739.
- Moriceau, C., and L. Fleitout (1989), A directional analysis of the small wavelength geoid in the Pacific Ocean, *Geophys. Res. Lett.*, *16*, 251–254.
- Neumann, G. A., D. W. Forsyth, and D. Sandwell (1993), Comparison of marine gravity from shipboard and high-density satellite altimetry along the mid-Atlantic ridge, 30.5°–35.5°S, *Geophys. Res. Lett.*, *20*(15), 1639–1642.
- Parker, R. L. (1973), The rapid calculation of potential anomalies, *Geophys. J. R. Astron. Soc.*, *31*, 447–455.
- Phipps Morgan, J. (1997), The generation of a compositional lithosphere by mid-ocean ridge melting and its effect on subsequent off-axis hotspot upwelling and melting, *Earth Planet. Sci. Lett.*, *146*, 213–232.
- Phipps Morgan, J., W. J. Morgan, Y.-S. Zhang, and W. H. F. Smith (1995), Observational hints for a plume fed, suboceanic asthenosphere and its role in mantle convection, *J. Geophys. Res.*, *100*, 12,753–12,767.
- Raddick, M. J., E. M. Parmentier, and D. S. Scheirer (2002), Buoyant decompression melting: A possible mechanism for intraplate volcanism, *J. Geophys. Res.*, *107*(B10), 2228, doi:10.1029/2001JB000617.
- Richter, F. M., and B. Parsons (1975), On the interaction of two scales of convection in the mantle, *J. Geophys. Res.*, *80*, 2529–2541.
- Robinson, E. M., B. Parsons, and M. Driscoll (1988), The effect of a shallow low-viscosity zone on the mantle flow, the geoid anomalies and the geoid and depth-age relationships at fracture zones, *Geophys. J. R. Astron. Soc.*, *93*, 25–43.
- Sandwell, D. T., and Y. Fialko (2004), Warping and cracking of the Pacific plate by thermal contraction, *J. Geophys. Res.*, *109*, B10411, doi:10.1029/2004JB003091.
- Sandwell, D. T., and W. H. F. Smith (1997), Marine gravity anomaly from Geosat and ERS-1 satellite altimetry, *J. Geophys. Res.*, *102*, 10,039–10,054.
- Sandwell, D. T., and W. H. F. Smith (2005), Retracking ERS-1 altimeter waveforms for optimal gravity field recovery, *Geophys. J. Int.*, *163*, 79–89.
- Sandwell, D. T., E. L. Winterer, J. Mammerickx, R. A. Duncan, M. A. Lynch, D. A. Levitt, and C. L. Johnson (1995), Evidence for diffuse extension of the Pacific plate from Pukapuka ridges and cross-grain gravity lineations, *J. Geophys. Res.*, *100*, 15,087–15,099.
- Scheirer, D., K. C. Macdonald, D. W. Forsyth, S. P. Miller, D. J. Wright, M. H. Cormier, and C. M. Weiland (1996), A map series of the southern East Pacific Rise and its flanks, 15S to 19S, *Mar. Geophys. Res.*, *18*, 1–12.
- Scheirer, D. S., D. W. Forsyth, M. H. Cormier, and K. C. Macdonald (1998), Shipboard geological indications of asymmetry and melt production beneath the East Pacific Rise near the MELT experiment, *Science*, *280*, 1221–1224.
- Shen, Y., D. W. Forsyth, D. S. Scheirer, and K. C. Macdonald (1993), Two forms of volcanism; implications for mantle flow and off-axis crustal production on the west flank of the southern East Pacific Rise, *J. Geophys. Res.*, *98*, 17,875–17,889.
- Smith, W. H. F., and D. T. Sandwell (1997), Global sea floor topography from satellite altimetry and ship depth soundings, *Science*, *277*, 1956–1962.
- Stoffers, P., T. Worthington, R. Hekinian, S. Petersen, M. Hannington, and M. Tuerkay (2002), Silicic volcanism and hydrothermal activity documented at Pacific-Antarctic Ridge, *Eos, Eos Trans. AGU*, *83*, 301–304.
- Tarantola, A., and B. Valette (1982), Generalized nonlinear inverse problems solved using the least squares criterion, *Rev. Geophys.*, *20*, 219–232.
- Toomey, D. R., W. S. D. Wilcock, J. A. Conder, D. W. Forsyth, J. D. Blundy, E. M. Parmentier, and W. C. Hammond (2002), Asymmetric mantle dynamics in the MELT region of the East Pacific Rise, *Earth Planet. Sci. Lett.*, *200*, 287–295.
- Turcotte, D., and G. Schubert (2002), *Geodynamics*, 456 pp., Cambridge Univ. Press, New York.
- Watts, A. B. (1978), An analysis of isostasy in the world's oceans: 1. Hawaiian-Emperor seamount chain, *J. Geophys. Res.*, *83*, 5989–6004.
- Watts, A. B. (2001), *Isostasy and Flexure of the Lithosphere*, 458 pp., Cambridge Univ. Press, New York.
- Weeraratne, D., D. W. Forsyth, and S. Webb (2003a), Rayleigh wave tomography study of the oceanic upper mantle beneath intraplate volcanic chains west of the East Pacific Rise, *Eos Trans. AGU*, *84*(46), Fall Meet. Suppl., Abstract V12B-0581.
- Weeraratne, D., E. M. Parmentier, and D. W. Forsyth (2003b), Viscous fingering of miscible fluids in laboratory experiments and the oceanic mantle asthenosphere, *Eos Trans. AGU*, *84*(46), Fall Meet. Suppl., Abstract V21B-03.
- Wessel, P. (1992), Thermal stresses and the bimodal distribution of elastic thickness estimates of the oceanic lithosphere, *J. Geophys. Res.*, *97*, 14,177–14,193.
- Wessel, P., and W. H. F. Smith (1991), Free software helps map and display data, *Eos Trans. AGU*, *72*, 441.
- Wessel, P., D. Bercovici, and L. W. Kroenke (1994), The possible reflection of mantle discontinuities in Pacific geoid and bathymetry, *Geophys. Res. Lett.*, *21*, 1943–1946.
- Wessel, P., L. W. Kroenke, and D. Bercovici (1996), Pacific plate motion and undulations in geoid and bathymetry, *Earth Planet. Sci. Lett.*, *140*, 53–66.
- Winterer, E. L., and D. T. Sandwell (1987), Evidence from en-echelon cross-grain ridges for tensional cracks in the Pacific plate, *Nature*, *329*, 534–537.
- Yale, M. M., D. T. Sandwell, and W. H. F. Smith (1995), Comparison of along-track resolution of stacked Geosat, ERS-1, and TOPEX satellite altimeters, *J. Geophys. Res.*, *100*, 15,117–15,127.
- Yamaji, A. (1992), Periodic hotspot distribution and small-scale convection in the upper mantle, *Earth Planet. Sci. Lett.*, *109*, 107–116.
- Zaraneck, S. E., and E. M. Parmentier (2004), The onset of convection in fluids with strongly temperature-dependent viscosity cooled from above with implications for planetary lithospheres, *Earth Planet. Sci. Lett.*, *224*, 371–386.

D. W. Forsyth and N. Harmon, Department of Geological Sciences, Brown University, Providence, RI 02865, USA. (nicholas_harmon@brown.edu)

D. S. Scheirer, U.S. Geological Survey, MS 989, 345 Middlefield Rd., Menlo Park, CA 94025, USA.